WL-TR-96-3080

HOPKINSON BAR PERFORATION OF LAMINATED GRAPHITE/EPOXY COMPOSITE

SYLVANUS N. NWOSU, PH.D.

HIGH ENERGY IMPACT RESEARCH LABORATORY
DILLARD UNIVERSITY
2601 GENTILLY BLVD
NEW ORLEANS LA 70122

MAY 1995

INTERIM REPORT FOR 12/10/93-12/31/94

FLIGHT DYNAMICS DIRECTORATE
WRIGHT LABORATORY
AIR FORCE MATERIEL COMMAND
WRIGHT PATTERSON AFB OH 45433-7562

DISCLAIMER NOTICE

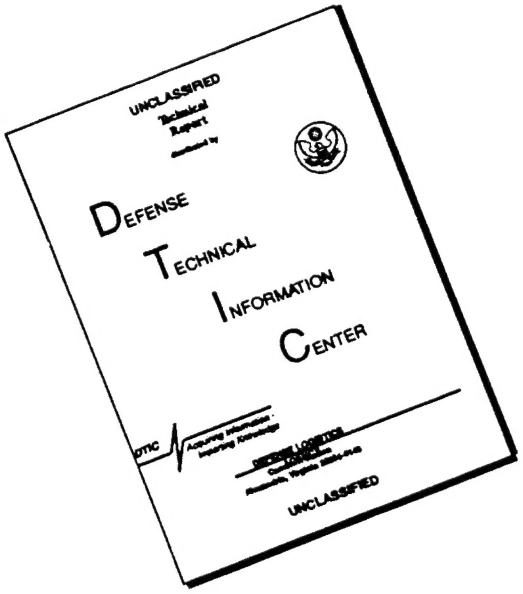

THIS DOCUMENT IS BEST QUALITY AVAILABLE. THE COPY FURNISHED TO DTIC CONTAINED A SIGNIFICANT NUMBER OF PAGES WHICH DO NOT REPRODUCE LEGIBLY.

NOTICE

When Government drawings, specifications, or other data are used for any purpose other than in connection with a definitely Government-related procurement, the United States Government incurs no responsibility or any obligation whatsoever. The fact that the government may have formulated or in any way supplied the said drawings, specifications, or other data, is not to be regarded by implication, or otherwise in any manner construed, as licensing the holder, or any other person or corporation; or as conveying any rights or permission to manufacture, use, or sell any patented invention that may in any way be related thereto.

This report is releasable to the National Technical Information Service (NTIS). At NTIS, it will be available to the general public, including foreign nations.

This technical report has been reviewed and is approved for publication.

Gregory J. Czarnecki

CZARNECKI, GREGORY J.
Program Manager
Survivability & Safety

Richard E. Colclough, Jr.

COLCLOUGH, RICHARD E. JR.
Chief
Vehicle Subsystems Division

James Hodges

HODGES, JAMES
Chief
Survivability & Safety

If your address has changed, if you wish to be removed from our mailing list, or if the addressee is no longer employed by your organization please notify WL/FIVS , WPAFB, OH 45433-7605 to help us maintain a current mailing list.

Copies of this report should not be returned unless return is required by security considerations, contractual obligations, or notice on a specific document.

REPORT DOCUMENTATION PAGE

Form Approved
OMB No. 0704-0188

1. AGENCY USE ONLY (Leave blank)	2. REPORT DATE	3. REPORT TYPE AND DATES COVERED
	May 10, 1995	Interim-12/10/93-12/31/94

4. TITLE AND SUBTITLE

HOPKINSON BAR PERFORATION OF LAMINATED GRAPHITE/EPOXY COMPOSITE

5. FUNDING NUMBERS

F33615-93-C-3411
PE 62201
PR 2402
TA 02
WU TV

6. AUTHOR(S)

Sylvanus N. Nwosu, Ph.D.

7. PERFORMING ORGANIZATION NAME(S) AND ADDRESS(ES)

High Energy Impact Research Laboratory
Division of Natural Sciences, Dillard University
2601 Gentilly Blvd, New Orleans, LA 70122

8. PERFORMING ORGANIZATION REPORT NUMBER

9. SPONSORING / MONITORING AGENCY NAME(S) AND ADDRESS(ES)

Flight Dynamics Directorate
Wright Laboratory
Air Force Material Command
Wright Patterson AFB, OH 45433-7562

10. SPONSORING / MONITORING AGENCY REPORT NUMBER

WL-TR-96-3080

11. SUPPLEMENTARY NOTES

12a. DISTRIBUTION / AVAILABILITY STATEMENT

APPROVED FOR PUBLIC RELEASE; DISTRIBUTION UNLIMITED

12b. DISTRIBUTION CODE

13. ABSTRACT *(Maximum 200 words)*

A Dillard University split Hopkinson pressure bar (SHPB) test apparatus was developed for dynamic quantification of energy expenditure in the perforation process of composite laminates. This report describes the basic features of the Hopkinson bar system for wave propagation and perforation experiments to characterize the perforation process, the nature of energy absorption process, and to explain and predict the extent of damage sustained during high strain rate perforation. Preliminary results for graphite/epoxy laminates show that the nature of energy expended in the perforation process depends on the thickness of the laminate, the fiber lay-up, the impact parameters and the incident stress delivered to the composite. The mode of laminate failure can be characterized by the level of energy absorption. The average impact energy per ply needed for damage initiation in graphite/epoxy were 7±1 J/ply, 10 J/ply and 11 ±3 J/ply for crack initation on the rear surface, perforation and plug push-out, respectively. The reflected stress waves show the presence of multiple peaks, possibly caused by reflection from the incident bar/indentor interface (due to the impedance mis-match at the interface). Although such reflection has a neglegible effect on the results, the indentor will be modified to eliminate this anomaly.

14. SUBJECT TERMS			15. NUMBER OF PAGES
Hopkinson bar, pressure bar	Dynamic impact	Stress wave, strain wave	78
Energy absorption	Perforation and penetration	Delamination	16. PRICE CODE

17. SECURITY CLASSIFICATION OF REPORT	18. SECURITY CLASSIFICATION OF THIS PAGE	19. SECURITY CLASSIFICATION OF ABSTRACT	20. LIMITATION OF ABSTRACT
Unclassified	Unclassified	Unclassified	SAR

PREFACE

This annual report was prepared by Dr. Sylvanus N. Nwosu, Associate Professor of Physics and Project Director of Dillard University High Energy Impact Research Laboratory. The report covers progress from 93 Dec 10 to 94 Dec 31 on the "Hopkinson Bar Perforation Impact and Mixed Mode Delamination of Laminated Plate" project funded by the US Air Force Wright-Patterson Air Force Base under contract # F333615-3-C-3411.

The author is especially indebted to Dr. Piyush K. Dutta for his suggestions and design of the Hopkinson bar facilities. The supports of Dr. Arnold Mayer and Mr. James Hodges to move this project forward is greatly appreciated. The author also expresses his profound gratitude and appreciation to Mr. Greg Czarnecki for close monitoring of the project objectives, experimental tasks, reviewing of the report and making excellent and constructive suggestions. Special thanks to Mr. John Kalafut for his assessment and evaluation of the instrumentation. The assistance of Mr. Suresh Sivapuram and all personnel at CRREL for their hard work in the design and initial testing of the Hopkinson bar apparatus is appreciated. The author greatly appreciates Dr. James J. Prestage, Chairman, Division of Natural Sciences, Dillard University, for his inspiration and encouragement through out the implementation of this program. The project has benefited from the continuous collaboration among Dillard University, the University of New Orleans (with Dr. David Hui) and the Cold Region Research and Engineering Research Laboratory (with Dr. Piyush Dutta).

TABLE OF CONTENTS

LIST OF ILLUSTRATIONS

LIST OF TABLES

HOPKINSON BAR PERFORATION OF LAMINATED GRAPHITE/EPOXY COMPOSITE

Sylvanus N. Nwosu

1. INTRODUCTION

The proposed work deals with Hopkinson bar experiments on laminated plates where the kinetic energy is sufficiently large to perforate the plate. The qualifier "Hopkinson", originated from pioneering impact tests on materials performed by a British physicist, B. Hopkinson (1914). By impacting a long cylindrical bar on one end with a projectile, a compressive stress wave pulse was generated at the impacted end. The incident wave propagated along the bar and was reflected at the opposite free end as a tensile stress wave. In conventional applications due to the extended work of Kolsky (1949,1953), two bars are commonly used. Referred to as a split Hopkinson bar, the sample to be tested is sandwiched between the incident and transmitter bars. Other researchers (Dutta et al. 1987, 1991) have applied the Hopkinson bar method for high strain rate testing of materials at cold temperature.

The proposed tasks under this contract have two technical objectives:

1. The design and application of the Hopkinson bar apparatus for perforation experiments and quantification of energy expended in the perforation process.
2. An investigation of the relationship between fracture surface morphology and the rate at which failure occurs.

The purpose of this report is to present completion of the first objective. When a projectile velocity approaches the ballistic limit velocity, the majority of energy is dissipated in the form of damage generation. Our interest is to understand the wave propagation phenomenon which causes plate damage and to characterize the damage mode. Compared to the conventional (ballistic) projectile experiment, the Hopkinson bar is ideal for examining the effects of projectile (indentor) velocity and the resulting stress wave on the damage of laminated plates near the ballistic limit. With the low velocity penetration afforded by a Hopkinson bar, the damage process can be better controlled, and it is possible to quantify the damaging stress wave using a digital oscilloscope. Materials can be penetrated at a precise location with no projectile deflection (in contrast to ballistic experiments).

Hopkinson bar experiments are designed to investigate strain rate sensitivity and are able to incorporate strain rate and stress wave effects in the perforation process. As such, Hopkinson

bar experiments differ considerably from static tests that have no strain rate effects, Charpy and Izod tests that do not account for stress waves and ballistic tests in which the stress waveform is difficult to measure. The Hopkinson bar method is less expensive and more reliable for studies of complex anisotropic and heterogenous systems such as composites. The mode of failure for such systems is complex and determined by several energy absorbing mechanisms operative during the perforation process. Within a certain energy range, it is possible that the damage mechanism is dependent on energy absorbed by the sample. Within other energy ranges, the damage mechanism may be governed by the striker velocity.

For the purpose of this investigation, the damage mechanism of a composite specimen, due to the penetration of an indentor, is accomplished in three successive stages of *indentation*, partial *penetration*, and *perforation* (complete penetration). Indentation is characterized by a small crater or indentation localized at the contact point with no visible crack on the exit side. The indentor may rebound with no penetration or dent sustained by the plate. The partial *penetration* stage involves entrance of the indentor into the plate and is characterized by formation of a deeper crater on the entrance side and with visible cracks and bulging on the exit side (Zhu et al. 1992). The penetration process increases the number of damaged fibers which results in a decreased resistance of the plate to damage. *Perforation* on the other hand is a complete penetration of the indentor through the plate characterized by punch-through and plug formation (where visible light can be seen through the plug hole). Embedment of the indentor increases and causes a further decrease in the plate resistance. Initiation of the punch-through and plug formation stage of perforation is when the tip of the indentor emerges from the plate. In terms of failure or fracture of the composite, such perforation is characterized by further global growth of the bulge, matrix cracking, fiber failure, plug push out, and delamination. Thus, depending on the impact conditions (impact energy, indentor geometry, or impact load), the indentor may rebound from the plate (resulting in no penetration), penetrate the laminate, or perforate it with plug formation. Since indentation and perforation are special cases of the penetration process, we will generalize the process as penetration with specific reference to perforation.

The penetrating process should be differentiated from conventional *impact* (short time duration loading). In contrast to actual impact between the striker and the incident bar, the SHPB penetrating head (the indentor) is already in contact with laminate before the test. The indentor

penetrates through the laminate by the impact between the striker and the bar. No impact occurs between the indentor and the laminate. Damage occurs by energy transfer during the penetration or perforation process.

The ultimate aim of the project is to achieve a perforation close to *ballistic limit velocity* (the threshold velocity necessary to just achieve a perforation). To accomplish this, the split Hopkinson bar system is modified by attaching a conical hemispherical-nosed indentor to the incident bar, while a fixture holding the laminated circular plate to be tested is attached to the transmitter bar. Since the objective is to test for the response of the laminates to impulsive loading during the penetration process, it is necessary that the indentor or incident bar emerge undamaged as a result of its encounter with the test materials.

A high stress level is generated along the bar from a longitudinal impact between a striker and the bar. The duration of the impact lasts for a few hundred microseconds (round-trip time of elastic longitudinal wave in the striker bar), and it takes a small time for the stress wave to enter and propagate through the test laminate at the opposite end of the incident bar. The impact results in development of a high compressive stress along the bar and a reflecting compressive wave (tensile stress) along the bar-laminate interface. Failure can be initiated if the combination of incident stress intensity and duration exceeds a critical value for the laminate [Zukas et al.1992]. The test specimen (and holding fixture) is sandwiched between the incident bar (with a hemispherically nosed indentor attached at the free end) and the transmitter bar. The mechanical behavior of the specimen determines the shape of reflected and transmitted pulses. Thus, the specimen properties (in general) can be characterized in terms of density and stress reflectance of the wave forms measured from the strain gages [Nwosu et al. 1994].

Kinetic energy delivered to the incident bar provides the driving force necessary for indentor penetration, which is achieved due to the bar's high mass and low velocity as compared to ballistic impacts.

2. TEST APPARATUS AND INSTRUMENTATION

The experimental set-up for the perforation system consists of (1) a **stress generating system** comprised of the striker driven by compressed air and the split Hopkinson bar, (2) a **test plate perforation fixture** that consists of the specimen holder and the indentor, (3) a **stress measuring system** made up of sensors, (typically resistance strain gages and PVDF sensors), and **(4) a data acquisition and analysis system**. Each component of the system is described below.

2.1 Stress Generating System

Figure 1 is the design layout of the split Hopkinson pressure bar (SHPB) photographed in Figure 2. The SHPB apparatus is comprised of incident and transmitter bars made of cylindrical maraging steel rod (300 maraging AMS 6414 steel) of 0.0254 m (1-in) diameter and 3.66 m (12 ft) length, and a striker bar having an identical diameter and 0.305 m (1 ft). The striker is housed inside a 0.610 m (2 ft) launch cylinder (see Figure 3). The striker is a piston, driven by compressed air of up to 1.72 MPa (250 psi). The compressed air reservoir is of high volume so that the desired pressure is maintained at constant air volume. A full-function automatic motor activates the compressor to recharge the reservoir whenever the pressure drops below 230 psi.

To begin each test, the desired pressure is set by a gauge between the launch cylinder and the air reservoir. A switch in the control room activates a quick-acting solenoid to open and allow the compressed air to accelerate the striker down the launch cylinder to impact the incident bar. Thus, the driving force of the striker is the potential energy of the gas converted to the kinetic energy of the striker. The impact end of the striker is spherically rounded with a 0.0508 m (2 inch) radius for a repeatable point of contact with the incident bar and on a plane centrally normal to the longitudinal direction of the wave propagation. Proper axial alignment between the striker and incident bars is maintained to minimize the generation of flexure. Uniaxial wave forms generated in the bar also determine the rate at which energy is transferred from the bar to laminated plate. The shape of the wave form is controlled by the geometrical shape of the striker and the impact velocity. The stress wave amplitude varies with impact velocity, while the stress profile changes with striker geometry [Dutta 1968].

As shown in Figures 1 and 2, the incident and transmitter bars are each guided through four pillow blocks with low friction ball bearings allowing only $\pm 1^0$ misalignment. The ball

bushings support the bar shaft without restraining it. The bars run longitudinally through the low friction ball bushing supports mounted on a 127 mm (5-inch) steel channel. The support can be adjusted laterally and vertically for proper alignment. To assist alignment and system stability, the channel and bars are mounted on a long rigid 0.165 m x 0.203 m (6.5" x 8") I-beam mounted on a 0.610 m x 0.610 m x 9.75 m (2' x 2' x 32') structural stand designed for maximum rigidity. The entire system is installed on the third floor of Stern Hall at Dillard University. To minimize vibration, the structural stand (Figure 2) is anchored on steel beams running through a 102 mm (4 in) steel reinforced concrete deck. A vibration test was performed on the system at the end of the installation and to certify rigidity. There was no detectable vibration within the sensitivity and trigger level of the sensor used for both the vibration test and the wave form measurements.

The impact launch cylinder and absorber components are pictured in Figure 3. A 6.35 mm (0.25-inch) diameter rod is attached to one end of the striker and protrudes outside the cylinder as a means of adjusting the stroke length or striker displacement. Two 19.1 mm (0.75-inch) diameter holes in the front side of the striker provide a means of venting the air inside the cylinder to the atmosphere and to provide a lower pressure zone in front of the striker. These holes also provide the means of venting the driving air at the end of the launch cylinder to prevent multiple impacts by the striker. A 7.62 mm (0.3-inch) tolerance between the striker's Teflon bearing and inside cylinder was enough to provide close fit, yet minimize air leaks and friction.

2.2 Test Plate Perforation Fixture

Figure 4 shows a schematic of the perforation assembly for the Hopkinson bar system. The figure shows the indentor and specimen support that holds the laminated plate. The fixture is sandwiched between the incident and transmitter bars as shown in Figure 5. The indentor is attached to the end of the incident bar through its inner diameter. The inside of the indentor is slightly recessed in to allow for complete contact with the incident bar. The sample holder fixture is attached to the transmitter bar with its open end facing the indentor. The space between the end of the fixture and the back side of the test plate allows for complete penetration or perforation beyond the thickness of the plate and without reaching the end of the fixture. [Note: In experiments performed near and beyond the perforation threshold (ballistic limit) the indentor punched through and impacted the end of the steel fixture resulting in damage to the indentor. The design has been modified and will be presented in future reports].

2.3 Stress Measuring System

The stress measuring system consists of resistance strain gages supplied by Measurement Group, Inc. The bridge for the gage is formed by two active diametrically opposing gages bonded to the mid-point of each bar. (The two gages are needed in order to cancel any bending that may result from bar misalignment.) The gages are connected into a four-arm, full-bridge configuration using a three wire technique. The gages' four-arm bridge completion is achieved with two 350-ohm fixed resistors. The bridge completion circuit is connected to a Micro Measurement amplifier which provides bridge balance through its internal bridge completion resistors and a bridge excitation of 12 V. A double shunt calibration circuitry was used to determine the total system gain and to reduce the sizable effect of lead wire resistance. Without an MTS machine, calibration of the system (to measure gage performance) has been indirect and needs some improvement. Figure 6 shows the electronic diagram necessary to measure the stress pulse. Following the application procedure recommended by Measurement Group, Inc., gages were bonded with M-Bond 200 at room temperature. An external trigger circuit uses a 6 volt battery to initiate the test by electrical contact between the striker and the incident bar (Figure 3).

2.4 Data Acquisition System

The data acquisition system is a Nicolet Pro 42 digital oscilloscope. Incident and reflected waves are sampled and recorded in channel 1 and the transmitted wave in channel 2 at a sampling rate of 20 million samples per second. The system has 12 bit digital resolution and a storage capability of 250,000 samples per channel. The scope is IBM DOS compatible and stores data on floppy disks. The recorded waveforms are shown in Figure 7. The analysis is accomplished by a Nicolet Spectrum Analyzer, capable of converting the data to Lotus and Excel formats. A consistent data manipulation technique was developed to handle data analysis.

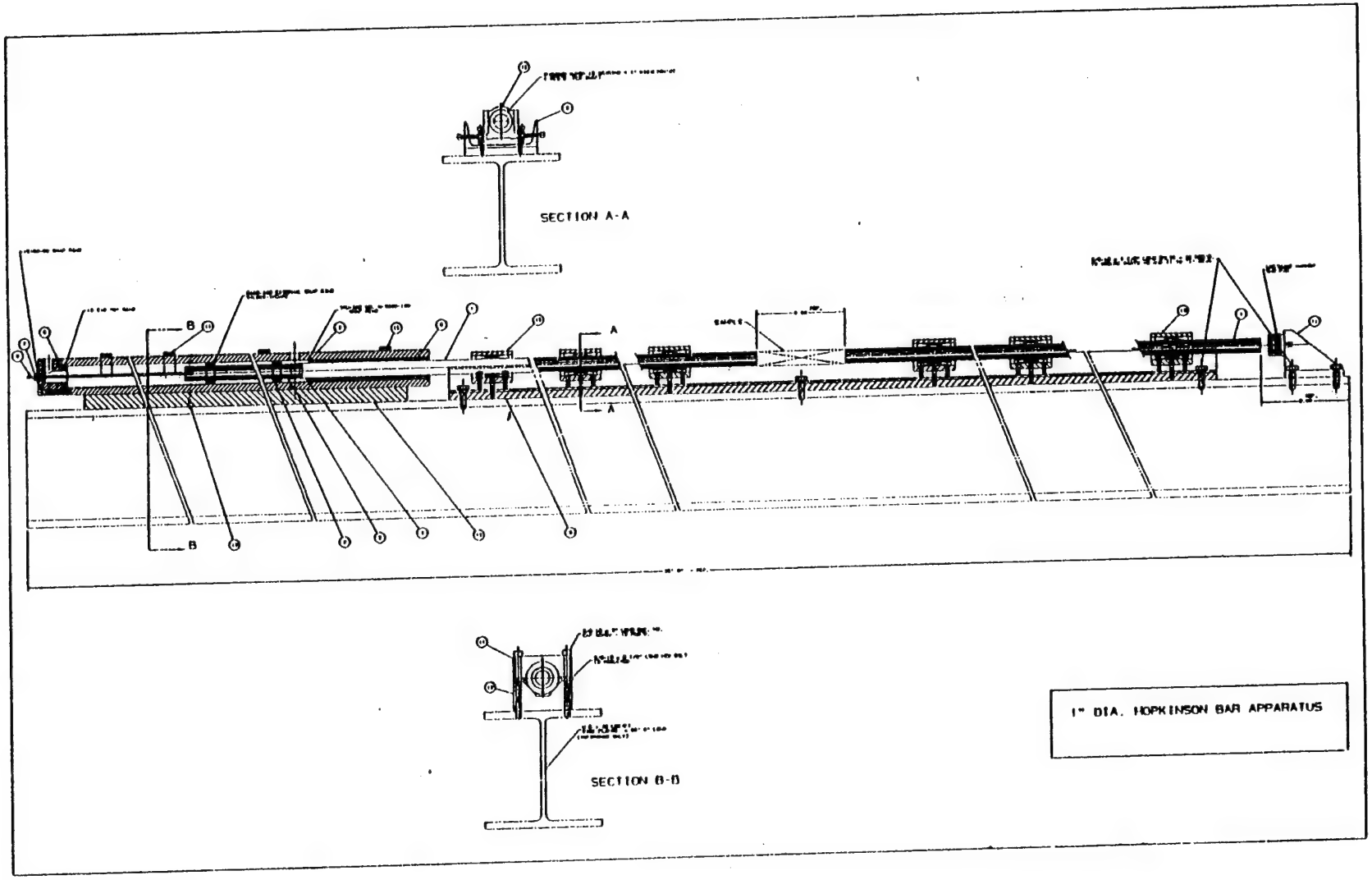

Figure 1. Schematic diagram of split Hopkinson bar system.

High-Performance Split Hopkinson Bar System (A)
and Pillow Ball Bearing Support (B)

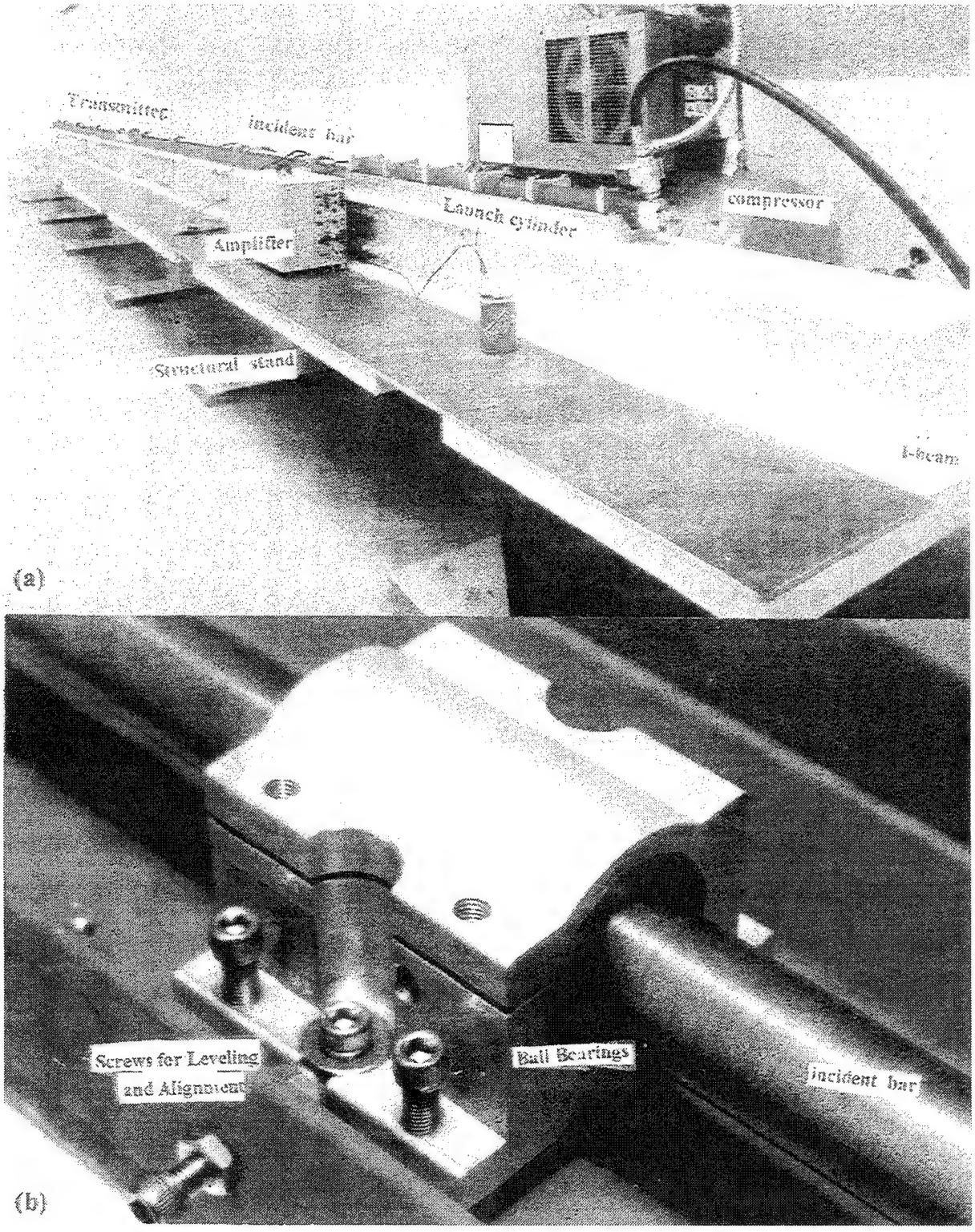

Figure 2. Dillard University high-performance split Hopkinson bar.

Launch Cylinder (A) and Impact Absorber (B)

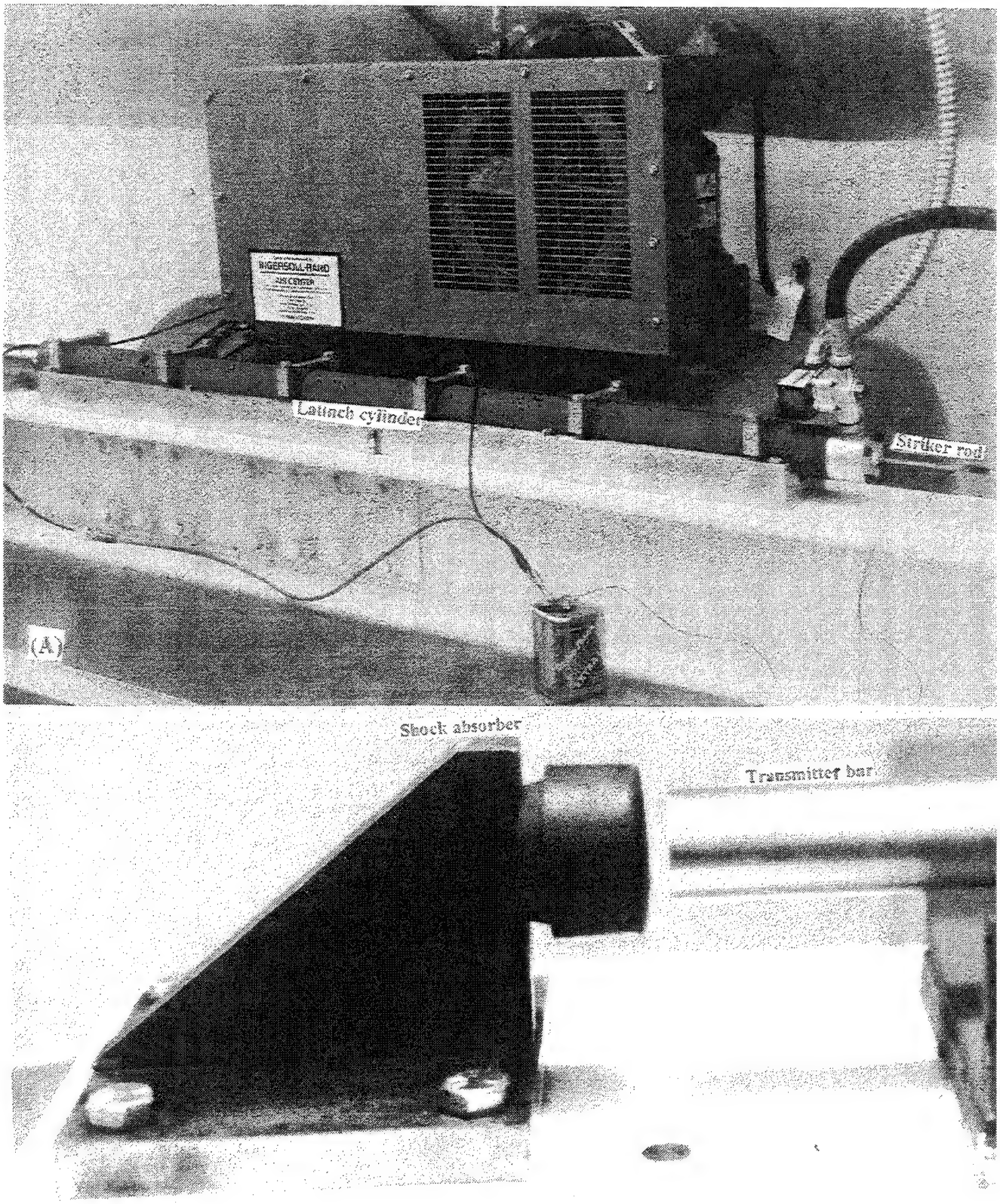

Figure 3. Launch cylinder and impact system

Plate Penetration Assembly showing Indentor and Graphite/Epoxy Support

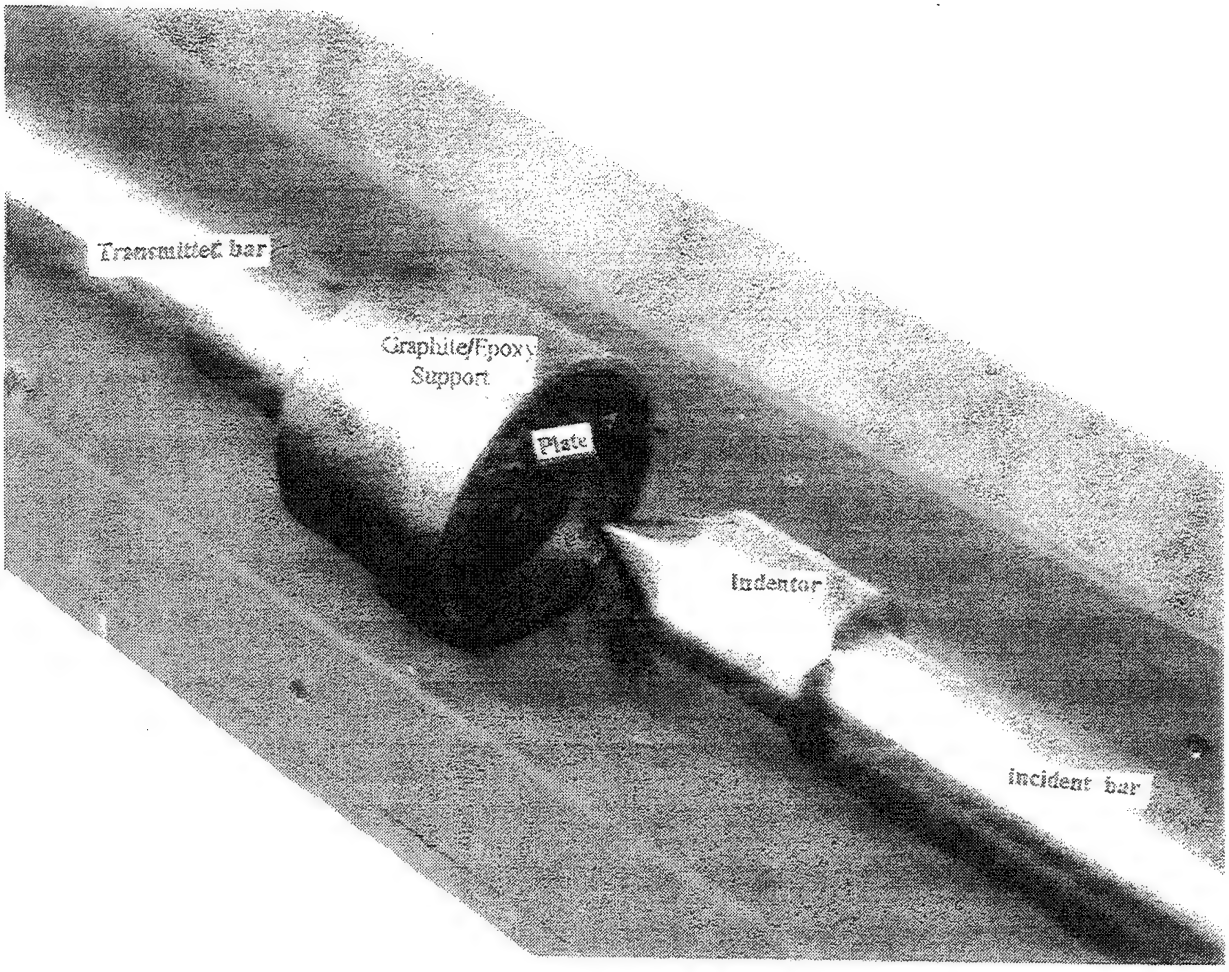

Figure 4. The test plate perforation fixture.

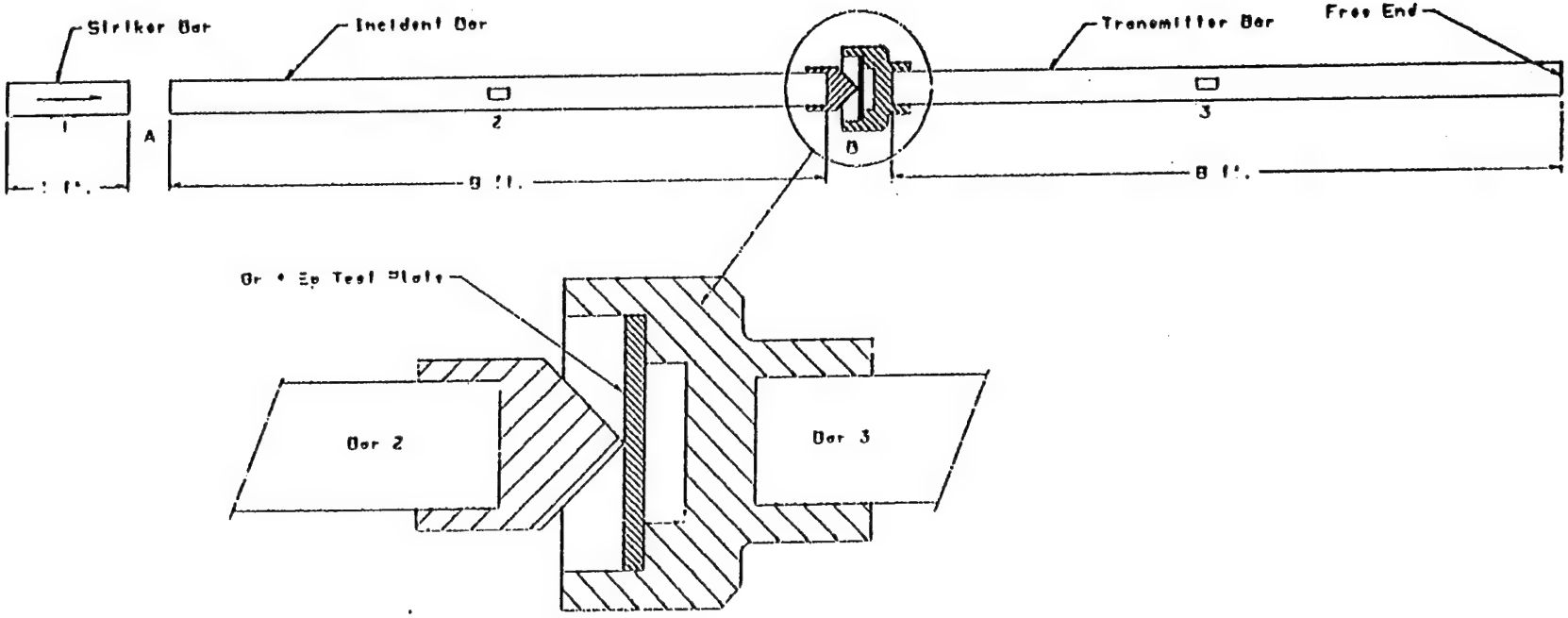

Figure 5.. Penetration fixture assembly showing indentor and fixture load with graphite/epoxy plate.

Bridge Circuit

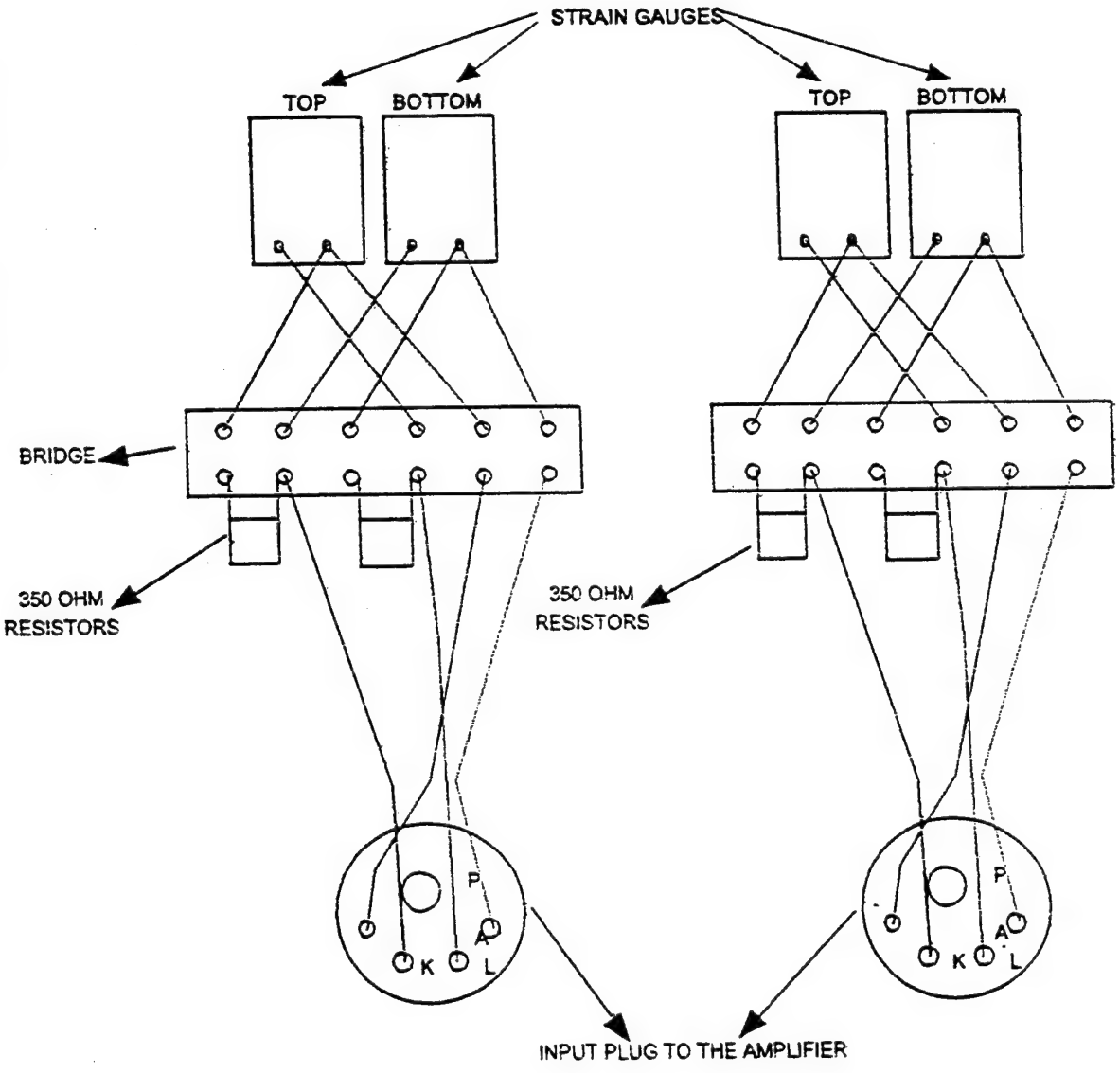

Figure 6. Schematic diagram of electronics set-up.

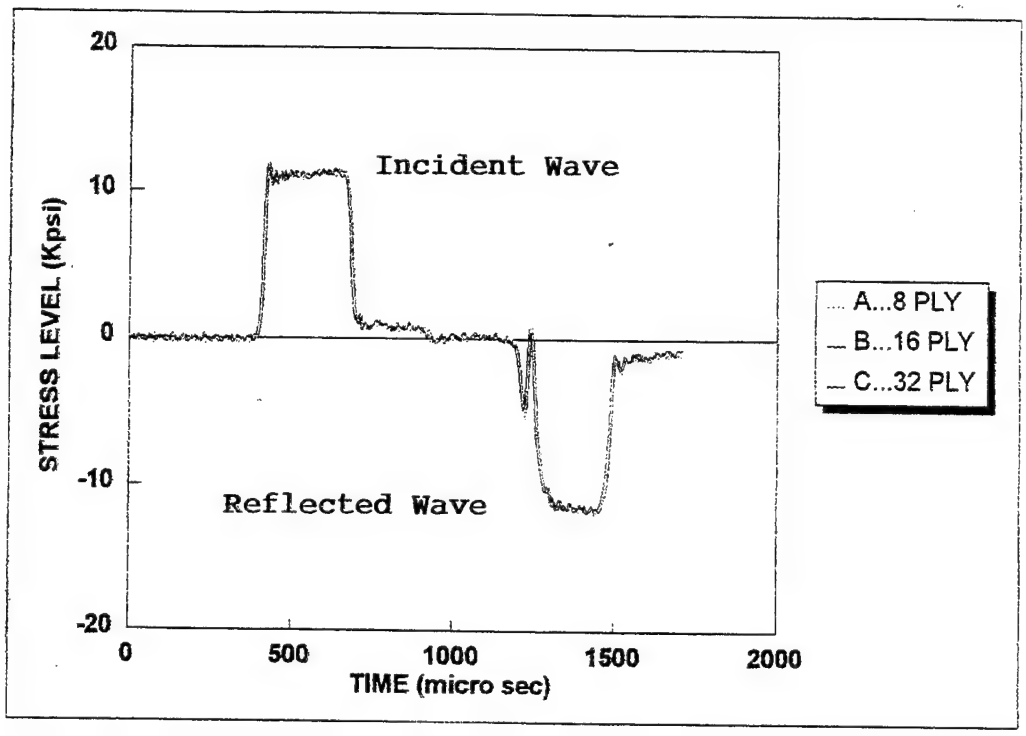

(a)

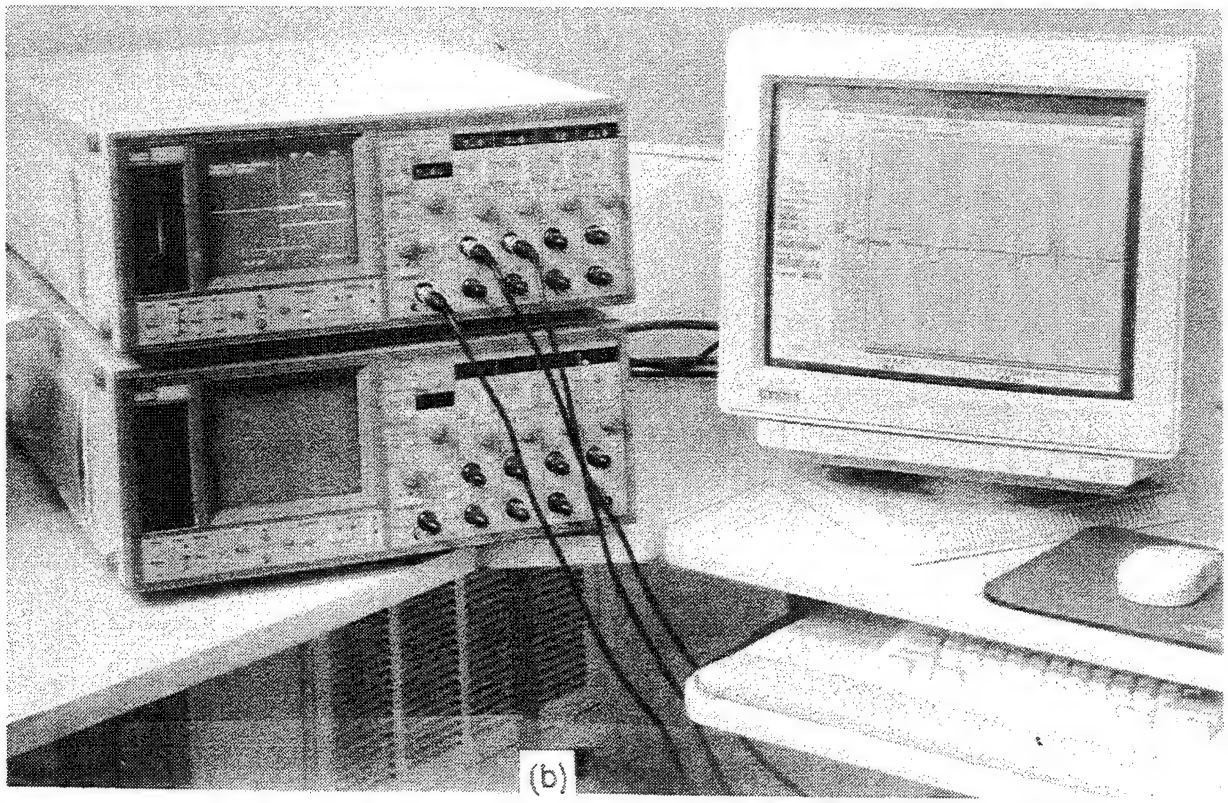

Figure 7. (a) Condition of incident stress level for 8-, 16-, and 32-ply graphite/epoxy samples (b) data acquisition system.

3. THEORY OF OPERATION

3.1 Basic Concepts

A mechanical wave in a solid is created by a localized mechanical disturbance that propagates from one section to another. For the present investigation, the disturbance is dynamic and characterized by a change in particle velocity and variation in physical quantities such as stress and strain that contribute to the time dependent description of the system. The mechanical wave of interest is generated by a rapidly varying boundary condition caused by the striker impact on a cylindrical solid bar.

Of primary importance in this study is the characterization of the damage process and its dependence on the materials and impact properties. The strength of a material, for example, is related to the maximum stress that it can withstand. The stress wave pulse propagates with a wave velocity that is characteristic of the medium through which it propagates. During propagation, particles that make up the medium undergo displacement from their equilibrium positions depending on the nature of the wave. The wave is considered transverse if the particle's motion is perpendicular to the direction of propagation. For a longitudinal wave, the particle displacement is along a line that is parallel to the direction of wave propagation. Since maximum stress is directly proportional to maximum particle velocity, they are important experimentally and can be determined from the stress wave data. An axial compression wave in a rod is approximately longitudinal when Poissons effect and the associated radial particle velocity are negligible.

Wave characteristics depend on the boundary conditions. When a propagating mechanical wave reaches a boundary that is neither free, nor fixed (e.g. the boundary between two dissimilar materials, as in this investigation), a portion of the incident wave is reflected due to an impedance mis-match between the boundaries. The remainder of the wave will be transmitted. For a free boundary surface, a compressive incident wave is reflected as a tension wave, and vise versa. If the interaction is at a fixed boundary, a compressive or tension wave is reflected as compression or tension wave with no change in shape, phase, or intensity. A detailed review of wave theory is presented by others (Zukas et al. 1992 and Graff 1975). Only an outline pertinent to the present investigation is included below.

Important assumptions for mathematical description of material deformation under

dynamic impact are as follows [Kolsky 1953, Bickle 1970]:

1. The composite plate is elastic and its properties remain unchanged by the impact.
2. The state of the stress over the cross sectional area is one-dimensional and uniaxial.
3. The wave is non-dispersive
4. The state of the stress at any instant is homogenous and in equilibrium over the entire composite plate.
5. Transverse strain, lateral inertia, and body forces are all negligible

Assumption 1 allows one to use the elementary wave theory to describe wave propagation within the composite. Neglecting minor local heating of the specimen, the material properties will remain unchanged throughout the penetration process. If d and L are the diameter and length of the bar, respectively, Poisson's effect is negligible when the Poisson's ratio is small compared to unity. (For compression, the Poisson's ratio is the ratio of fractional lateral elongation ($\Delta d/d$) to fractional axial contraction ($\Delta L/L$) of the bar). Elementary wave theory that neglects Poisson's effects are valid for the description of wave motion in a SHPB if the wavelength (λ) of a propagating waves is ten times the diameter (d) of the bar (Bickle 1970). In the present investigation, the wavelength of the incident pulse is 610 mm compared to 25.4 mm of rod diameter. Thus, elementary wave theory is valid.

A one-dimensional uniaxial state of the stress is necessary. Otherwise, the wave will deviate from a planar wave to a non-planar wave having a curved front. The planar condition is satisfied by making the bars prismatic and slender. Such a plane wave will remain planar and parallel to the cross section as it propagates from one section to the other. If L is the bar length traveled by the wave, the condition of one-dimensional planar state of the stress is satisfied if the slenderness ratio $d/L < 1/50$ [Zukas et al. 1992]. Our test apparatus has a slenderness ratio of 1/144. Thus, any deviation of the wave motion from a one-dimensional and planar state is negligible. The striker generates a long pulse (122 μs) which will be discrete and planar for a 365 μs travel time before being interfered by a returning wave.

A wave is dispersive if it changes shape (or has some components that travel at different velocities) without losing energy (in contrast to attenuation where the wave loses energy). Issues rated to the effect of dispersion in a SHPB at high strain rate are worthy of verification because composite materials undergo elastic deformation under dynamic or non-uniform loading

conditions, making it possible for the pulse to change in amplitude and duration after transmitting through the specimen. Since the axial stress in the specimen depends linearly on the axial strain on the transmitter bar, dispersion could result in underestimating the strength of the materials. However, the rate of dispersion is small and negligible when the *rise time* (the time required for the stress to increase from 10% to 90% of its final value) of the stress pulse is two or three times greater than the time required for the pulse to traverse the diameter of the rod. The theoretical rise time is given as

$$\tau_{10/90} \approx 1.96 \nu^{2/3} (L/d)^{1/3} \left(\frac{d}{\sqrt{E/\rho}} \right) \qquad (1)$$

where L is the wave propagation distance, d is the diameter of the rod, and ν is the Poisson's ratio [Bickle 1970]. For our experimental set-up, the rise time for the incident wave pulse is 15 μs compared to 5 μs to traverse the diameter of the rod (three times greater). Following a recent estimate by Ravichandran and Subhash (1994), the effect of dispersion is minimized if $(r/\lambda) > 0.1$, where r is the radius of the bar. Using Rayleigh's approximation and defining the frequency of the propagating input wave or its Fourier component in terms of phase velocity, the frequency of the input pulse f (η) can be written as

$$f(\eta) = f_0 [1 - (\nu\pi)^2 \eta^2] \qquad (2)$$

where $f(\eta)$ is taken as an integral multiple of fundamental frequency of pulse in the bar, $f_0 = C_0/r$ and $\eta = r/\lambda$ [Zukas et al. 1992]. For our SHPB setup where r, C_0, and ν values are 12.7 mm, 5010 m/s, and 0.3 respectively, and using $\eta = 0.1$, dispersion is minimized if f (η) is at least $0.99 f_0$, or if the period or duration of the input pulse is at least 2.6 μs ($f(\eta) = 3.91 \times 10^5\ s^{-1}$) Comparatively, the input pulse duration for our SHPB is 122 μs . Rayleigh's approximation also shows that within 1% error, the wave can be assumed to propagate with its fundamental frequency, f_0 ($3.95 \times 10^5\ s^{-1}$).

The state of the stress wave in the specimen is homogeneous if the wave travel time through the specimen is small compared to the duration of the incident wave. Since the wave velocity through a graphite/epoxy composite is about 8467 m/s, the transient time (t_0) required to

traverse a 32-ply (for example) is 4.3 μs, which is short compared to 122 μs for duration of the incident wave. The stress will be homogeneous within the specimen when the time to equilibrate (τ) is αt_0, where α is the number of multiple reflections within the specimen [Ravichandran and Subhash (1994)]. With the short transverse time of 4.3 μs, several multiple reflections are possible such that the state of a wave within the specimen will be homogenous as shown in the Lagrangian diagram in Appendix E. The effects of non-uniform stress and non-equilibrium within the short specimen used in this study are also minimized by using longer bars (longer wavelengths). Assumption 5 is satisfied since the impact is normal to the longitudinal direction and an axial compression is generated in the bar. Lateral expansion is negligible since the condition on rise time is satisfied.

3.2 Mathematical Formulation

For a typical experiment, the striker of length S_L is pulled back in the cylinder to a stroke length of S_s. A set pressure *(p)* is applied at one end of the striker. The impact stress or release of the striker is controlled by a solenoid valve such that when the valve is opened, stored potential energy of the compressed air accelerates the striker over a displacement, S_s. Neglecting any losses in energy along the ram, the change in the kinetic energy of the striker is equal to the net work done by the applied force (pA), so that, the impact velocity of the striker in terms of applied air pressure can be written as

$$V_0 = \sqrt{\left(\frac{2p}{\rho}\right)R} \tag{3}$$

where $R = S_s/S_L$ is the ram ratio, and ρ is the density of the striker.

The longitudinal impact load F_0 of the striker acts for a time dt on a section dx of mass m and cross sectional area A. From Newton's second law,

$$F_0 dt = mV_0 = (\rho A dx)V_0 \tag{4}$$

The impact generates a compressive stress wave pulse that propagates through the bar. From equation 4, the initial compressive stress on the bar is given as

$$\sigma_o = \frac{F_0}{A} = \rho C_0 V_0 \tag{5}$$

where $C_0 = dx/dt$, is the bar wave velocity. Using equation 3, the initial stress can be expressed in terms of impact and bar parameters as

$$\sigma_0 = \frac{E_0}{C_0} K\sqrt{pR} \tag{6}$$

where $\rho C_0 = E_0 / C_0$. The value K is a conversion factor equal to 0.0158 $(m/kg)^{1/2}$ for pressure (p) in Pascal or 1.31 for p in psi, and the ram ratio $R = S_s/S_L$ is a dimensionless constant. The amplitude of the wave pulse depends on the impact velocity (a function of the applied air pressure), the ram ratio and material properties of the striker. The greater the ram ratio, the higher the impact energy. The kinetic energy of the indentor is equal to work done by the indentor compressive load (neglecting energy losses) such that the work-energy relation can be written as

$$\frac{1}{2} m_b V_{pb}^2 = \int_0^{\delta} P(y) dy \tag{7}$$

where V_{pb} is the indentor penetrating velocity, δ is the maximum penetration or perforation depth, and $P(y)$ is the indentor contact force for perforation. The functional dependence of $P(y)$ on depth of penetration y can be estimated from the area under the force-displacement curve. Contact law [Zukas et al. 1992] can be written for all the regions of the loading and unloading [Tan et al. 1985] and used to estimate the perforation velocity. This is the subject of further investigation to be presented in future report.

The particles in the incident bar will propagate to the right at a relative velocity of V_b in the longitudinal direction of the wave pulse. We adopt the convention that: (1) particle velocities are positive when they are in the same direction as the associated propagating wave and 2) the compressive stress are positive. At the incident bar/specimen boundary (Interface B), part of the wave pulse will be reflected back into the incident bar as a tensile wave pulse because of the impedance mis-match, while others will be transmitted through the specimen with a particle

velocity of V_s. For equilibrium at the interface (Figure 5), the continuity for force requires that

$$F_b=(\sigma_i+\sigma_r)_b A_b=F_s=(\sigma_t)A_s \tag{8}$$

and continuity of velocity at the interface implies

$$V_b=V_i-V_r=V_s \tag{9}$$

where from equation (5)

$$\begin{aligned} V_i&=\frac{\sigma_i}{(pC)_b}\\ V_r&=\frac{\sigma_r}{(pC)_b}\\ V_t&=\frac{\sigma_t}{(pC)_s} \end{aligned} \tag{10}$$

and $V_i = V_0$ at the striker-bar interface. The subscripts i, r, t are for incident, reflected and transmitted waves, respectively and the subscripts b and s refer to the bar and specimen, respectively. The minus sign is from the fact that reflected particle velocity is in the opposite direction upon reflection. Solving equation 9 using equation 10, the particle velocity transmitted into the specimen is written as

$$V_s=\frac{C_0}{E_0}(\sigma_i-\sigma_r) \tag{11}$$

and the transmitted and reflected stresses are expressed in terms of incident wave and mechanical impedance Z (where $Z= \rho CA=E_0A/C_0$) as

$$\sigma_t=\left(\frac{2Z_s(A_a/A_s)}{Z_s+Z_b}\right)\sigma_i \tag{12}$$

$$\sigma_r = \left(\frac{Z_s - Z_b}{Z_s + Z_b} \right) \sigma_i \qquad (13)$$

Equation 13 shows that a compressive wave is reflected in compression ($+\sigma_r$) if $Z_s > Z_b$, and in tension ($-\sigma_r$) if $Z_s < Z_b$. For impedance matching, $\sigma_r = 0$ since $(Z_s - Z_b) = 0$.

To determine the displacement or penetration of the particle at time t, consider X_i and X_t as positions associated with the ends of the incident and transmitter bars respectively. A sample of thickness L_s is sandwiched between the ends of bars. A compressive incident wave on arriving at the interface X_i is partially reflected (because of the impedance mis-match) and partially transmitted. The X_i interface is displaced by u_i (due to the incident wave) and u_r (due to the reflected wave). Thus, the net displacement of the X_i surface of the incident bar is given in equation 14 as

$$U_i(t) = u_i - u_r = \frac{C_0}{E_0} \int_0^t [\sigma_i(t) - \sigma_r(t)] \qquad (14)$$

Similarly, at the X_t interface the transmitter bar is displaced by u_t (due to the transmitted wave, neglecting the effect of the boundaries due to the specimen holder) such that the net displacement at X_t is expressed as

$$U_t(t) = u_t(t) = \frac{C_0}{E_0} \int_0^t \sigma_t(t) dt \qquad (15)$$

The net displacement in the sample is approximately equal to the penetration and is given as

$$U_i(t) - U_t(t) = u_n(t) = \frac{C_0}{E_0} \int_0^t [\sigma_i(t) - \sigma_r(r) - \sigma_t(t)] dt \qquad (16)$$

For a bar of cross sectional area of A, the instantaneous force, $F_i(t)$, exerted on the specimen by

the indentor and $F_t(t)$ exerted on the specimen by the transmitter bar are given respectively as

$$F_i(t)=A[\sigma_i(t)+\sigma_r(t)] \tag{17}$$

and

$$F_t=A\sigma_t(t) \tag{18}$$

The net energy produced by the indentor in penetrating the sample is

$$E_p=\int_0^t F_i(t)du_n \tag{19}$$

and can be obtained as the integrated area of the force-displacement curve over the wave's duration. Damage to the laminate occurs by the transfer of energy given by equation 19 during the penetration process. Neglecting energy losses within the fixture, the total energy absorbed by the specimen is the incident energy minus the reflected and transmitted energies through the specimen and expressed as

$$E_A=\left(\frac{AC_0}{E_0}\right)\int[\sigma_i(t)^2-\sigma_r(t)^2-\sigma_t(t)^2]dt \tag{20}$$

where $E = (AC_0/E_0)\int\sigma^2\,dt$ for incident (E_i), reflected (E_r) and transmitted (E_t) energies. Equation 20 is the total energy absorbed by the system and includes the energy lost by vibration, stretching of the plate, friction , and contact. For perforation, the indentor emerges through the plate of thickness, *a*, to height *h*. (As defined below, h is the distance the indentor travels beyond the plate in a punch through event or the height of the cone of the damaged area above the thickness of the plate). The total energy required to perforate (E_{perf}) the plate under dynamic conditions is expressed as:

$$E_{perf}=P_m\delta+E_p \tag{21}$$

where P_m is the average force over the duration of the perforation event and obtained from the integration of the force-time curve; E_p is the energy produced by the indentor necessary for penetration (from equation 19) and the term P_m δ is the additional energy required for punch

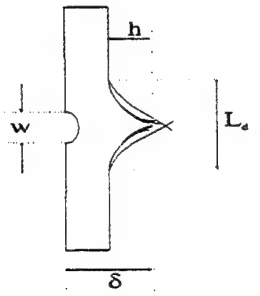

through, where δ = a + h.

The total energy required for perforation can also be predicted from the energy balance model by accounting for the energy absorbed (E_A) by all the competing processes (Shivakumar et al. 1985) during the perforation event as

$$E_A = E_c + E_b + E_f + E_e + E_v + E_x \tag{22}$$

where, E_c is the energy lost by the indentor during Hertzian contact, E_b is the energy lost by the plate due to bending, E_f is the energy lost by the indentor due to friction, E_e is the energy associated with elastic stretching, E_v is the energy associated with indentor vibrations, and E_x is the energy lost to the test fixture. Thus, the threshold (critical) impact velocity is approximately equal to the ballistic limit expressed as

$$V_{BL} = \sqrt{\left(\frac{2}{m_b} E_{perf}\right)} \tag{23}$$

where the bar mass, $m_b = (\rho AL)$ can be expressed in terms of density, cross sectional area and length of the bar. The change in kinetic energy of the bar and the associated residual velocity can

be expressed respectively as

$$\Delta E_r = \frac{1}{2} m_b V_{pb}^2 - E_{perf} \tag{24}$$

$$V_r = \sqrt{\frac{2}{m} \Delta E_r} \tag{25}$$

The residual energy, ΔE_r, can also be estimated as $(F_p h)$, where F_p is the average peak contact force for the duration of the perforation event and h is the height beyond the specimen thickness. A plot of residual velocity (V_r) versus perforation velocity (V_p) or striker impact velocity (V_i of equation 2) estimates the critical velocity. The critical impact (or perforation) velocity is the impact (or perforation) velocity when residual velocity is set to zero. Complete presentation of this will be presented in the final report.

The specimen's strain, strain rate and stress can be respectively expressed in equation 26 as

$$\begin{aligned} \varepsilon_s(t) &= \frac{-2C_0}{L_s} \int_0^t \varepsilon_r(t) dt \\ \frac{\partial \varepsilon_s(t)}{\partial t} &= \frac{-2C_0}{L_s} \varepsilon_r(t) \\ \sigma_s(t) &= \frac{A}{A_s} E_0 \varepsilon_t(t) \end{aligned} \tag{26}$$

where A and A_s are the cross sectional areas of the transmitter bar and specimen, respectively.

4. MATERIALS AND EXPERIMENTS

Each test specimen is a circular plate having a geometry and fiber lay-up as shown in Table 1. The plate is simply supported around a circular inner diameter of 2.0-in the perforation fixture and held in place by the indentor slightly pressed against it without stress. A rubber band was used to keep the indentor and sample in contact.

Targets tested in the present investigation consist of graphite/epoxy (Hercules toughened thermoset 8551-7A) material ranging from 8-plies to 32-plies. Each ply contains unidirectional continuous fibers. Thin targets were expected to flex and have damage (in the form of delamination) initiate at the rear surface (opposite the point of contact). Conversely, thick targets were expected to sustain extensive subsurface damage (local to the point of contact) and little flexure (Daniel et al. 1990). Experimental results indicate that increasing the thickness increases the resistance of the plate to perforation.

All laminates are unidirectional and subjected to transverse compressive load. This means that the load is perpendicular to the fiber direction. Studies have shown that transverse compressive load usually result in matrix shear failure, and matrix shear failure with constituent debonding and/or fiber crushing [Agarwal et al. 1979]. Thus, in the order of energy levels, damage can occur as minor matrix cracking, fiber breakage, delamination, penetration and perforation (or a combination of matrix cracking, fiber fracture, and delamination). The major experimental objective is to characterize the generation of damage during a penetrating process (indentation, penetration and perforation) in terms of energy expenditure and size of visible (surface) damage.

The following experiments were designed to accomplish the objectives:

A. Preliminary feasibility perforation impact test at CRREL.

B. Effect of laminate thickness on damage for a constant impact energy.

C. Effect of incident stress (impact energy) on energy absorbed for the same thickness.

D. Effect of impact energy on penetration with impact energy for different thickness.

E. Effect of fiber lay-up on the nature of damage generation for a constant thickness.

F. Effect of impact energy on energy absorbed for different thicknesses.

G. Interactions of two or more of the above parameters.

A consistent low noise technique was developed and used to measure the stress-strain history as a function of time during performance of the above experiments. The data analysis was achieved using a Nicolet Spectrum Analyzer and suitable software to obtain the following information:

1. Variation of stress and strain with time and displacement.
2. Contact force as a function of time.
3. Penetration and particle velocity variation with time.
4. Variation of size of surface damage (area, length of crack and size of surface indentation) as a function of test parameters.
5. Variation of energy absorbed with particle velocity, penetration, impact force, thickness, and fiber orientation.
6. Crack propagation as a function of impact velocity.

The response strain signal is measured in volts. Electronic double shunt calibration of the system indicated a conversion factor of 0.833 micro strain/mV or 171.8 MPa/mV (25,000 psi/mV) using Young's modulus (E_0) of 2.07 x 10^5 MPa (30 x 10^6 psi) for maraging steel. The strain pulse was measured as a function of time and converted to stress using $\sigma(t) = \varepsilon(t) E_0$. A calibration of the system under static and dynamic impact conditions of known force was not used in the present analysis because double shunt calibration data were obtained under uniform dynamic conditions.

TABLE 1

CHARACTERISTICS OF GRAPHITE/EPOXY SPECIMENS

Thickness	8-ply sample (GP1)	= 1.042mm (0.041in)
	8-ply sample (GP2)	= 1.042mm (0.041in)
	16-ply sample (GP3)	= 2.083mm (0.082in)
	32-ply sample (GP4)	= 4.064mm (0.160in)
	Specimen Diameter	= 617 mm (2.43 inches)

Lay-up	GP1	$[\pm 45]_{2s}$
	GP2	$[\pm 45/0/90]_{s}$
	GP3	$[\pm 45/0/90]_{2s}$
	GP4	$[\pm 45/0/90]_{4s}$

Experimental Data on Maraging Steel:

Young's Modulus of Maraging Steel	2.07×10^5 MPa (30×10^6 psi)
Wave Velocity in the Hopkinson Bar	5010 m/sec (16,437ft/sec)
Density of Maraging steel	8000 kg/m^3
Yield Stress of Maraging Steel	2.03×10^5 MPa (295×10^5 psi)

Impact Properties: Indentor is 3/16" hemispherical nosed maraging steel

Ram Ratio, R=1 (12" striker displaced through a 12" ram to impact)

Impact Energy (J) = 1.06 x Impact stress (in psi)

5. RESULTS AND DISCUSSION

5.1 Characterization of the Wave Forms

Figure 7(a) shows a typical measured stress signal for incident and reflected waves. An extreme similarity of the results (between 8, 16, and 32-ply samples) is noted when uniform impact conditions are applied. According to equation 6, the incident stress depends on the bar material, the length of the striker (S_L), the compressed air pressure (p) driving the striker, and the striker displacement, S_s (stroke length) before impact in the direction of wave propagation. However, the reflected wave (due to an impedance mis-match at the interface) depends on the interface and specimen properties, and suggests mechanical information about the materials defining the interface. The double reflected wave shown in Figure 7 is due to impedance mis-match at the bar/indentor interface and will be discussed later.

5.2 Damage Initiation and Penetration Process Stages

The results shown in Figure 8 illustrate the variation force, particle velocity, energy absorption, and penetration history for graphite/epoxy laminates with a conical hemispherical indentor. The complete penetration process involves three possible inter-dependent damage events: compression, shear plug formation, plug separation, delamination, and perforation (Zukas et al. 1992). The perforation is preceded by matrix cracks, crack growth and intersection, leading to debonding and delamination. These events are completed in the four penetration stages identified and discussed below. Plotted values are scaled for comparison purposes.

Stage I. Compressive Loading and Unloading Stage. This first stage is mainly compressive and corresponds to the initial loading. As the indentor decelerates into the plate, the contact force increases and the plate is pushed or flexed forward with increasing particle velocity and decreasing indentor energy. Similarly, energy absorbed by the plate (energy lost by indentor) increases very rapidly as the indentor transfers its kinetic energy to the plate. Damage in the form of crack formation can be initiated at the contact region depending on both the stress level and the

material's properties. This region commonly represents the fracture initiation site. The load increases during this stage resulting in a build up of elastic strain energy on the specimen. The force increases to a critical value at the end of the loading stage during which deformation may occur. Since the perforating velocity during this initial loading is greater than the forward velocity of the laminate, it is conceivable that matrix cracking and penetration are initiated depending on the threshold kinetic energy at which these events can occur. At the time of the peak force, it is possible that all of the available energy has been stored by the specimen and none remaining for damage initiation. No permanent damage such as delamination will occur in the laminate if the laminate stores all of the available perforation energy at the time the load returns to zero. This is because the indentor begins to rebound after this point and no energy is retained for damage propagation. We assume that the initial perforation energy is the sum of energy required for fracture initiation plus the energy required for fracture propagation. Thus, if all the energy is expended in fracture initiation, none will be available for its propagation and therefore major events such as perforation and punch through may not be reached.

As the indentor continues to decelerate, force applied to the laminate is reduced. A sudden decrease in impact load (contact force) is indicative of incipient damage (Sun et al. 1985). The plate may continue to flex forward causing a rapid drop in the contact force between the indentor and plate. This reduction in contact force is primarily caused by the presence of damage in the laminate. As the penetration increases, the force decreases as more fibers deform under the crushing of the indentor. Energy absorbed locally by the deforming plate becomes constant around the indentor as the failurein stage I reaches its outer boundaries. The peak energy is the maximum energy available for the perforation process (equation 19). In general, the point of maximum energy absorbed by the specimen is not necessarily the point of failure initiation. Incipient damage may be initiated before this point or not initiated at all.

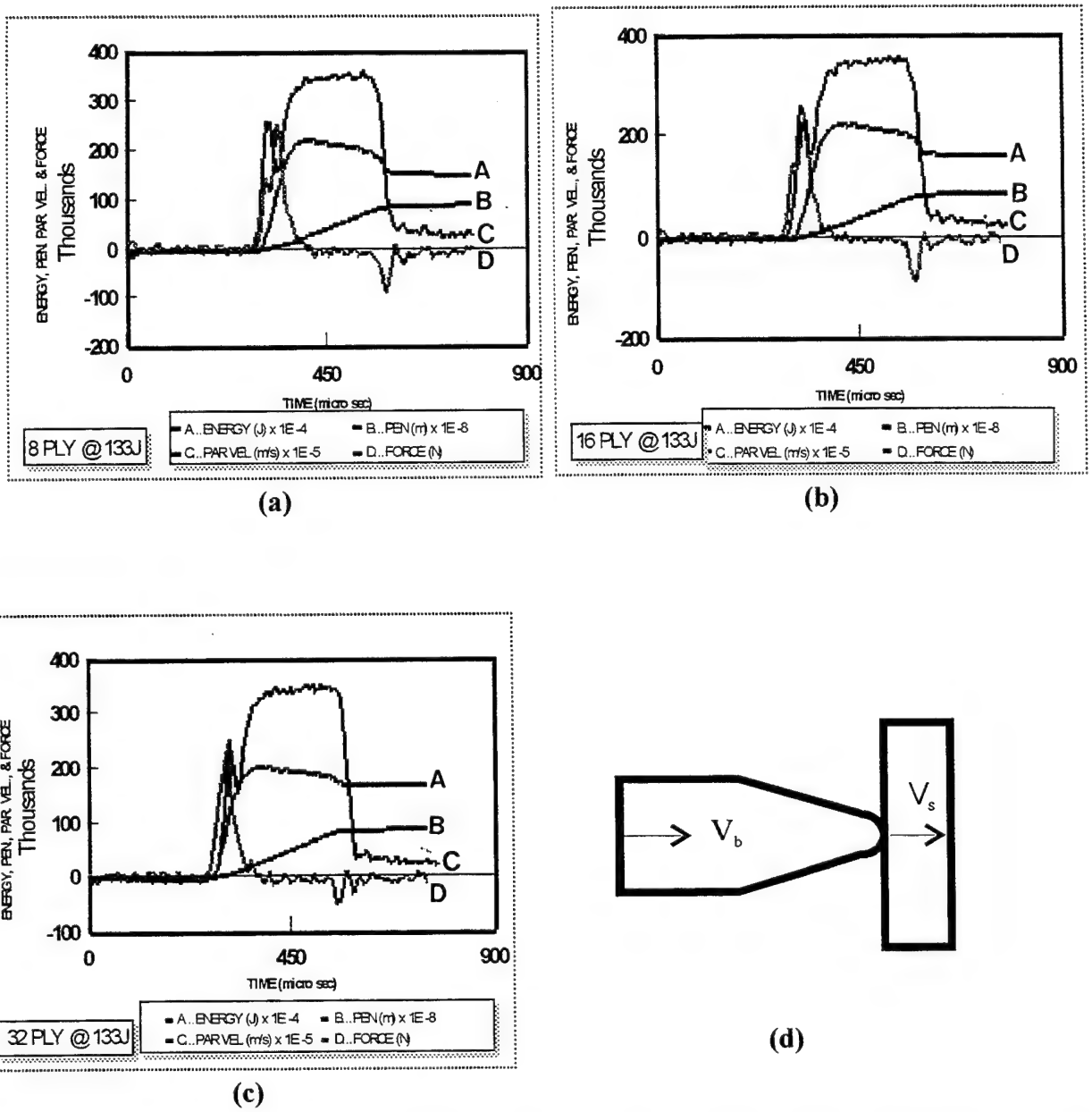

Figure 8. Energy, penetration, particle velocity and force history measurements of (a) 8-ply (b) 16-ply, (c) 32-ply graphite/epoxy laminates penetrated at 133J striker impact energy, and (d) indentor laminate interface. (Note: Energy (J) x 10^{-4}; Particle Velocity (m/s) x 10^{-5}; and Penetration (meters) x 10^{-8})

Stage II: Equilibrium Stage. Any crack or fracture created in stage I is propagated in a progressive manner during this stage. When the perforation velocity matches the forward motion of the laminate, a shear plug may form. Thus, the specimen can fail catastrophically. The energy absorption begins to attain a constant value corresponding to a constant particle velocity stage in which there is little or zero net contact force and the indentor's forward motion terminates. The constant velocity is also expected from the continuity condition at the bar-specimen interface (equations 9). It is important to note from Figure 8 that the propagation of the failure, penetration depth and energy absorbed all continue to increase even at loads of zero. This observation shows the rate effect of stress wave which continues to propagate with constant energy through the specimen even at zero contact force. The indentor continues to penetrate through the plate at almost constant particle velocity while the plate is held fixed by the perforation fixture. As the force provided by the indentor diminishes to zero, the indentor experiences some vibration . The slight vibration shown in the force diagram (Figure 8) results from the fact that thin plates bend and behave like a spring-mass system in the contact region.

Stage III: Reloading (Tensile Wave) Stage. The compressive wave now reaches the rear surface of the specimen and is reflected off as a tensile wave. This is indicated by the observed reversal of the force direction (in the force-displacement curve). This represents a tensile release force at the plate interface and acts normal to the laminate interface increasing from the rear surface to the impacted surface. This causes a sharp decrease in absorbed energy since the reflected energy is subtracted from the total energy. The decrease could also be the release of the elastic strain energy stored in the specimen during the loading stage. Czarnecki (1991) demonstrated that a tensile wave/compressive interaction zone exists for damage transitions from shear plugging to delamination. The tensile forces acted normal to the laminate and was identified as a potential source of delamination. It appears from Figure 8 that the dynamics of crack growth leads to a sudden unloading in the surface traversed by the crack front and emits tensile stress waves from the surfaces. The effect of such a tensile wave is to influence further motion of the crack, and delamination in the fiber direction increases progressively at the laminate rear surface. The energy absorbed and penetration continues to increase due to displacement of the indentor through the plate and propagation of the incident compressive wave. The velocity begins to drop

because of the rebound of the indentor and corresponding reflected wave. The absorbed energy will start to decrease at the beginning of the increasing tensile wave (because the total energy is the incident energy minus the sum of the reflected and transmitted energies). The laminate also returns some part of its residual or absorbed energy to the indentor after a major damage.

Stage IV: Vibration Stage. This stage involves the residual energy absorbed by the system. In this stage, indentor is stopped and the system assumes a state of constant residual energy. This energy includes the vibration energy due to oscillation of the indentor and the plate as shown in the force vs displacement curve. Studies have shown that the vibration mainly originates from elastic waves traveling back and forth in the impactor (Sjoblom et al. 1988) and that the amplitude of such vibration increases with impactor velocity.

5.3 Multiple Reflections due to Impedance Mis-Match at Indentor/Specimen Interface

Multiple reflections (double-peaks) observed in the results shown in Figures 8 and 9 warrant some discussion. The multiple reflections are caused by reflections due to impedance mis-match from the incident bar/indentor interface and indentor/specimen interface. Wu et al.(1994) measured the force history of the impact of a tipped striker on a thin aluminum plate using laser Doppler Anemometry and the observed double-peak phenomenon was attributed to the vibrating effect of the plate during impact. In the case of nonperforated impact, they proposed that the first peak represents the initial impact stage in which the projectile pushed the plate forward and the second peak is the result of rebound from the projectile when it can no longer push forward. The results indicate that near the ballistic limit, cracks occur in the contact region and the double peak disappears. Beyond the ballistic limit, the peak force remained constant and no double-peak phenomenon was observed. The studies concluded that the second peak force occurs when the indentor's final velocity is equal to zero and the double peaks phenomenon occurs when the projectile velocity is not high enough to produce incipient damage on the target. For the perforation of graphite/epoxy laminates presented, where the indentor is initially in contact with the plate, damage or penetration is caused by energy transfer as the indentor pushes forward through the plate. Thus, double impact from the indentor is not possible, although the plate and indentor could vibrate at the contact region due the incident compressive stress and

striker impact.

The results of a quasi-static punch-through test of graphite/epoxy strongly suggest that double peaks correspond to initiation of different damage mechanisms (Sun el al. 1993). With this in mind, the first peak may be identified as the onset of delamination induced by matrix cracks while the second peak corresponds to formation of a shear plug of the same diameter as the indentor. No visible damage may be seen ordinarily on the surface of the contact region or rear side. The second peak may indicate delamination, rear face fiber breakage, or shear plug formation. This plug is pushed out under a decreasing load which eventually attains a constant value [Sun et al. 1993, 94]. The second peak could also be part of the local reaction (resistance) force exerted on the indentor by the plate support. This results when the indentor can no longer push the plate forward in agreement with Wu et al. (1994). Under this situation, the plate has a tendency to rebound or recoil. At the rear exit surface, delamination is formed due to the reflected tensile wave and shows up as a second peak with greater amplitude because of greater damage area.

While we agree that different damage mechanisms could cause double peak phenomenon, it appears that the phenomenon observed in this report is mainly caused by a mechanism different from a damage mechanism or double contact. This is because the phenomenon was also observed in some cases where there was no detectable visible damage or internal damage to the laminate. We now postulate that the double peak phenomenon (double reflection) observed here is caused by an impedance mismatch between the indentor and the incident bar. To investigate this, a series of impact experiments (no penetration or perforation) were designed with the indentor attached to the bar free end and without contact with the laminate. The result in Figure 9 (a) shows the appearance of multiple reflections. The first reflection (shown by the arrow) is from incident bar/indentor interface since this is the only boundary interface encountered by the wave before reflection from the bar free end (second reflection). Figure 9(b) shows the result when the interface is eliminated by removing the indentor. The absence of a first reflection in Figure 9 (b) clearly demonstrates that the multiple reflection is occurring from an earlier reflection from the indentor/bar interface due to impedance mismatch between those interfaces.

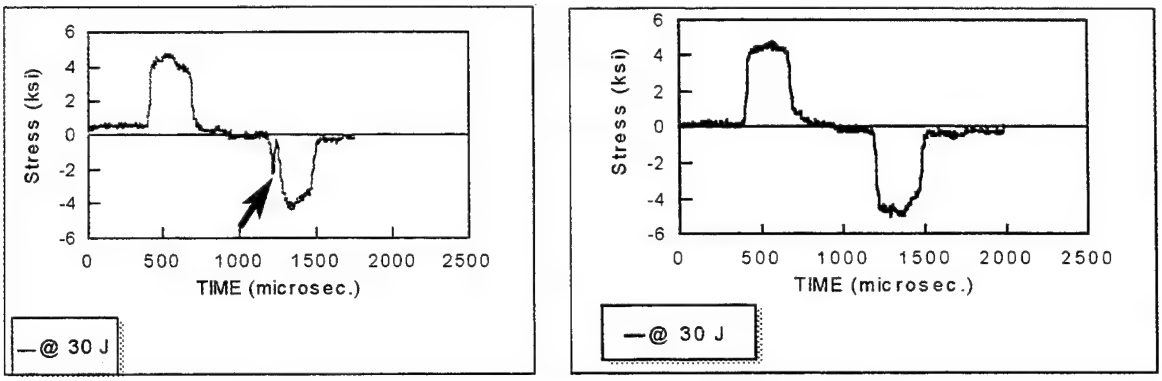

(a) **(b)**

Figure 9. (a) Reflection from incident bar/indentor interface without contact with the laminated plate and (b) absence of reflection when indentor is removed.

Because the indentor is attached to the incident bar through its inner diameter (see Figures 4 and 5), the first small reflection is due to an early reflection of the incident wave from the indentor's inner diameter interface with the incident bar. The reflection is small because of the slight impedance mismatch at the boundary possibly due to small change in cross sectional area. In Figure 8, the portion of the incident wave that reaches the laminate is heavily reflected back (causing the second reflection of greater amplitude) because of the higher impedance mismatch between the laminate and indentor. Delamination could also be a contributing factor to the multiple reflections and is further being investigated. In more recent studies [Nwosu et al. 1995], multiple peaks and greater distortion of wave occurred in penetration of laminate but absent in perforation. This is due to continuous damage and vibration caused by the embedded indentor inside the laminate without perforation. No such distortion is observed in perforation since the major event is punch-through and plug push out with most of the residual energy returning to the indentor. Thus, it is possible that the double peak phenomenon will disappear in that case as observed by Wu et al.(1994). One must be careful, however, not to equate damage generation in single homogenous aluminum plate with that of laminated composite plate.

5.4 Energy Absorbed vs Particle Velocity

Particle velocity and vontact force are is independent of laminate thickness but dependent on impact energy. The particle velocity transmitted through the specimen increases gradually with absorbed energy during the loading and unloading stage before attaining a constant at the maximum value. The results (Figure 10) show that the particle velocity is independent of laminate thickness but strongly depends on impact energy level (Figure 11). This is further explained in Figure 12.

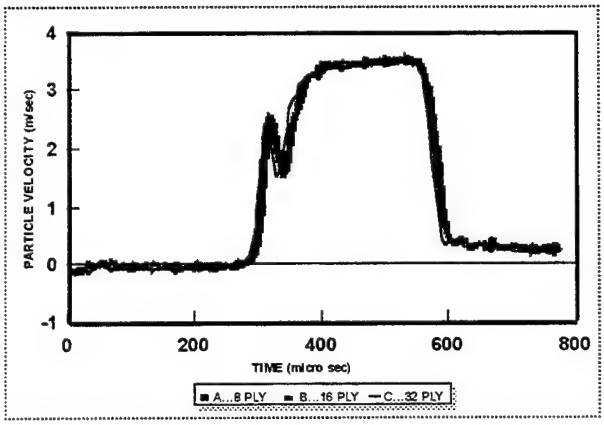

Figure 10. Particle velocity-time history for 8-, 16-, and 32-ply graphite/epoxy laminates using striker impact energy of 133 J.

5.5 Impact Energy vs the Total Deformation.

Compressive wave/tensile wave interaction zone is marked as the point when particle velocity and energy absorbed start to decrease. Figures 11 and 12 represent the variation of force and particle velocity versus penetration for 16- and 32-ply specimens penetrated at three impact energy levels. The results show that the peak force and penetration increase with impact energy level but remain independent of the specimen's thickness throughout the penetration process (Figure 12). This is because a particle's motion about its equilibrium position depends

mainly on the chemical (atomic) properties of its material and not on the material physical properties. The higher the impact energy, the greater the load on the bar and therefore the greater the disturbance or vibration of the particles.

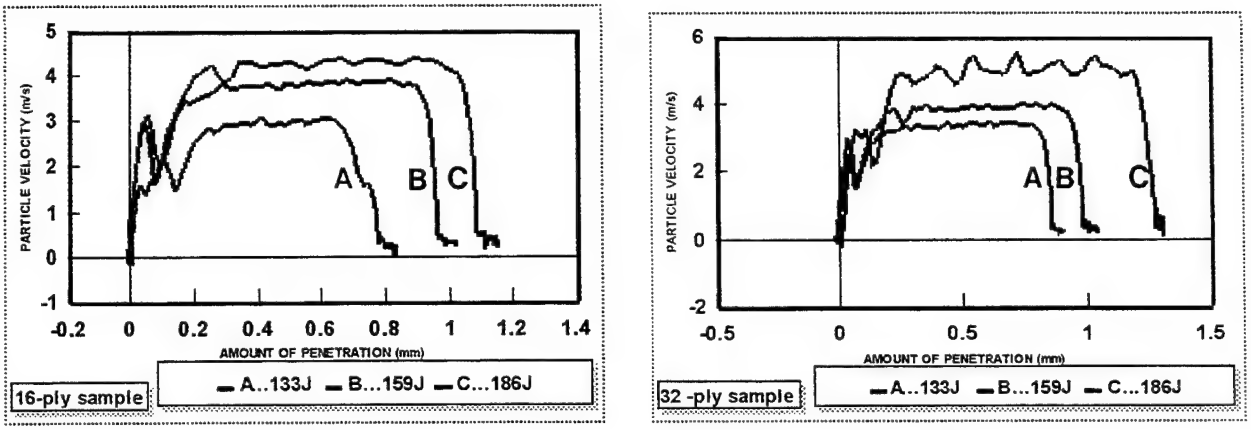

(a) (b)

Figure 11. Particle velocity variation with penetration for (a) 16-ply and (b) 32-ply graphite/epoxy laminates varying impact energies.

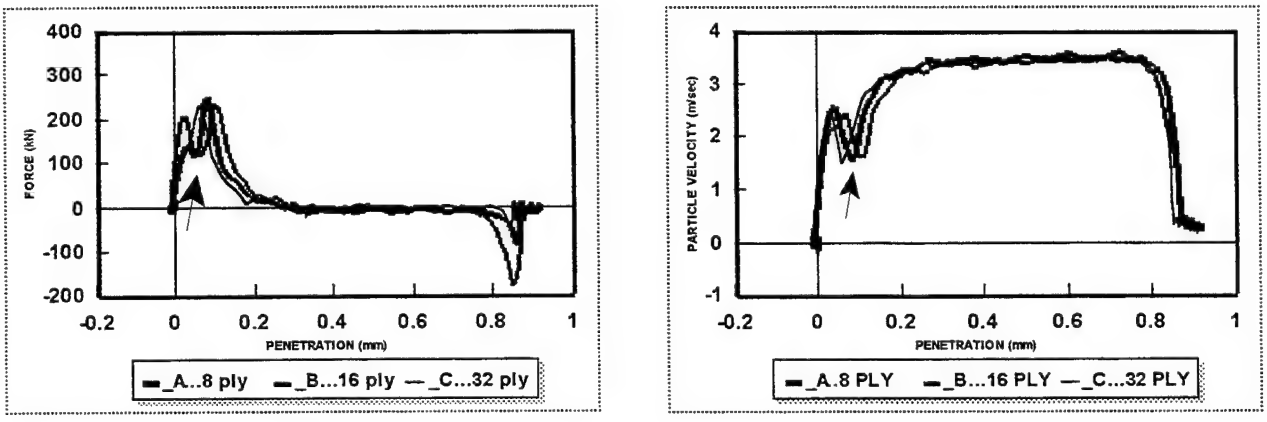

(a) (b)

Figure 12. (a) Force and(b) particle velocity variations with penetration for 8, 16, and 32-ply graphite/epoxy laminates at 133 J impact energy.

The ringing in the 32-ply laminate at 186 J (Figure 11) is an indication of greater vibration for the 32-ply sample resulting from greater residual energy than for the thin sample. Such vibration is less in the 16-ply sample that was perforated. Note the reversal of the particle velocity (shown by the arrow) due to the multiple reflection discussed earlier and the gradual decrease to zero at the end of the penetration process. The initial rapid increase in velocity with penetration occurs during the loading stage as the indentor accelerates through the plate. This is followed by the constant velocity stage, then a slower drop in velocity to zero at the end of the penetration. For the three incident stress levels, the measured penetration are 1.10 mm, 0.95 mm, and 0.82 mm for 186 J, 159 J, and 133 J, respectively for the 16 and 32-ply samples. Although the penetration increases with incident stress level, for a given impact energy the amount of penetration is identical for both thicknesses. While crack formation and damage can clearly be observed on 16-ply samples, none is observed on 32-ply samples below 233 J. It is conceivable that subsurface damage exists. This is presently being investigated by C-scan, deply, and SEM studies at the University of New Orleans.

The maximum particle velocity further indicates the velocity at which the indentor and plate move forward in unison in the incident direction. For plate velocities less than this value, the indentor accelerates into the plate with a contact force increasing positively with time [Dutta et al. 1991]. At the instant of penetration, the interaction between the indentor and plate is inelastic. However, because the plate is able to flex, its velocity relative to the indentor can be zero. If the plate velocity becomes greater than the indentor velocity, the indentor will lose contact or rebound, resulting in a tensile force near the laminate rear surface. The result in Figure 13 was achieved at low impact energy at 133 J. Only a dent was observed on the entrance side of the 32-ply sample. The force and perforation variations with time show that penetration through the plate increases with time. The force curve shows the characteristic initial rapid increase followed by a slower decrease to zero. Energy absorbed starts to decrease when the initial compressive force reflects back in tension. The variation of absorbed energy with time shows that although force and penetration are the same, the 32-ply sample absorbed more energy than the 16- and 8-ply samples although the total peak energy associated with 32-ply specimens was less than that of the thinner laminates.

The reflected force amplitude for 32-ply specimen's was also less than that of the thinner

specimens which shows that although the incident force can be the same (due to the same incident stress), the extent of damage differs with thickness. Penetration at the time of force reversal gives an estimate of the total deformation of the plate but not the nature of the deformation. The reflected stress wave form carries information about material properties and the nature of damage. From the results, it can be seen that the amplitude of the reflected compressive stress wave (tensile wave) in most cases decreases with sample thickness. This could be because most of the energy has been used in the damage process and less returned to the indentor. Comparison with post-test specimen photographs shows that samples with lower amplitude reflected waves suffer less rear surface cracking and fiber breakage. Maximum penetration and force release is reached after 650 μs. The time is independent of thickness but depends on the impact energy. The higher the impact force the greater the total energy transferred, and the higher deformation. The value of the absorbed energy (Figure 13 (c)) after this point gives a good estimate of the residual properties for the damage process. Figure 14 describes the variation of energy absorbed with penetration at three energy or stress levels. The absorbed energy increases with impact energy. The difference in peak energy for the 32-ply laminates is uniform compared to the 16-ply.

5.6 Effects of Laminate Thickness and Impact Energy on Energy Absorbed

Energy absorbed by the laminate depends on thickness and impact energy. In Figure 15, a linear relationship is described between energy loss of the indentor (net energy absorbed by the specimen) and peak penetration energy. The solid curve is a polynomial nonlinear fit to the experimental data. The fit assumes zero energy absorbed at zero initial force, velocity, and penetration for perforation. Peak energy is the maximum energy expended by the indentor and is obtained from the peak value in the energy vs time curve. Neglecting all the energy losses to the fixture, the peak energy is approximately the maximum indentor energy available for perforation. Some part of this energy will be lost to such damage mechanisms as vibration, friction, plastic deformation, etc. and the rest will be absorbed by the plate or returned to the indentor.

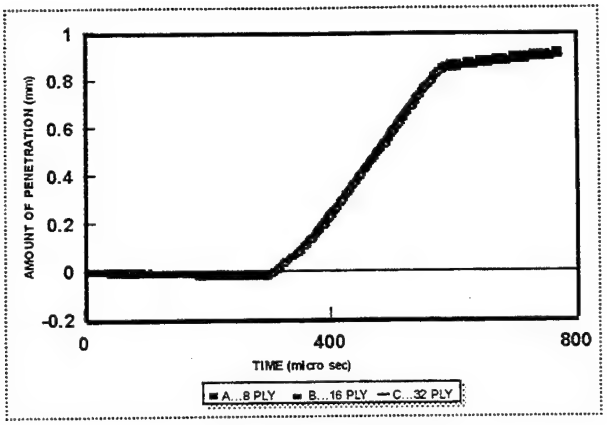

(a)

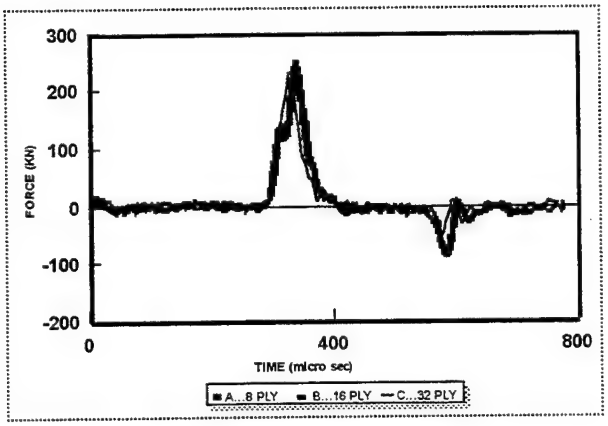

(b)

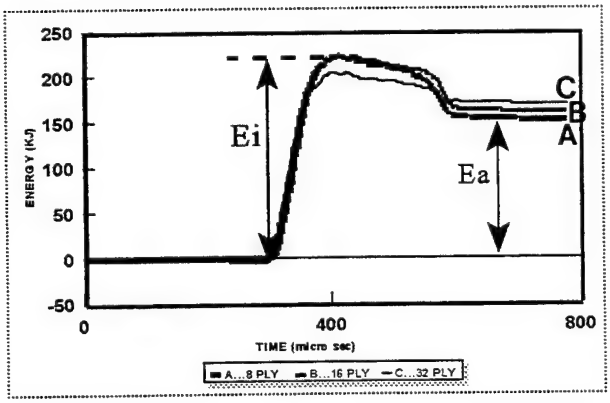

(c)

Figure 13. (a) Penetration, (b) force and (c) energy-time curves for various thicknesses at 133 J striker impact energy. (E_i=total energy input, E_a=energy stored, or absorbed by the laminate due to impact)

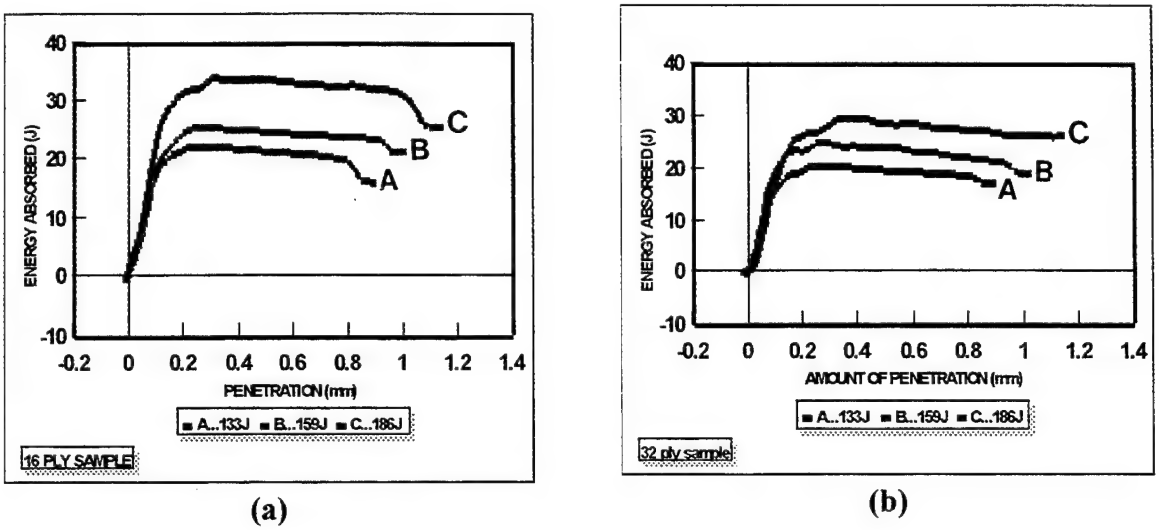

Figure 14. Energy absorbed vs penetration depth for (a) 16-ply and (b) 32-ply graphite/epoxy laminates at three impact energy levels.

5.7 Damage Process

Damage process is not a linear function of impact energy for all regions of the damage process. Figures 16(a-d) describe peak energy absorbed vs incident stress, peak force, penetration, and particle velocity, respectively. Tests were performed using a consistent launch velocity (equation 2). Although more experimental data are needed to confirm the observed trends, the relationship between energy absorbed, particle velocity, and amplitude of the incident stress as in Figures 16 (a-d) are quadratic during the initial stage and linear at a higher incident stress, particle velocity, and penetration. From wave propagation theory, energy transferred to the specimen is proportional to the square of the incident wave amplitude. As shown in Figure 16 (b), the higher quadratic term in the non-linear fit, shows that the relationship between energy absorbed and peak force is more linear for the 32-ply sample (without perforation) than the 16-ply samples (with penetration). The point of deviation appears to be an indication of transition to another damage mechanism, possibly from matrix cracking and fiber breakage or delamination and perforation. For the same impact conditions, the 16-ply laminate approaches the perforation threshold earlier than the 32-ply. After a perforation is achieved at the threshold kinetic energy for a 16-ply sample, the energy absorbed may deviate from linear variation of impact energy. Most of the energy, after the material failure, is returned to the indentor while energy absorbed by the specimen remains constant. This is equivalent to being outside of the specimen's elastic

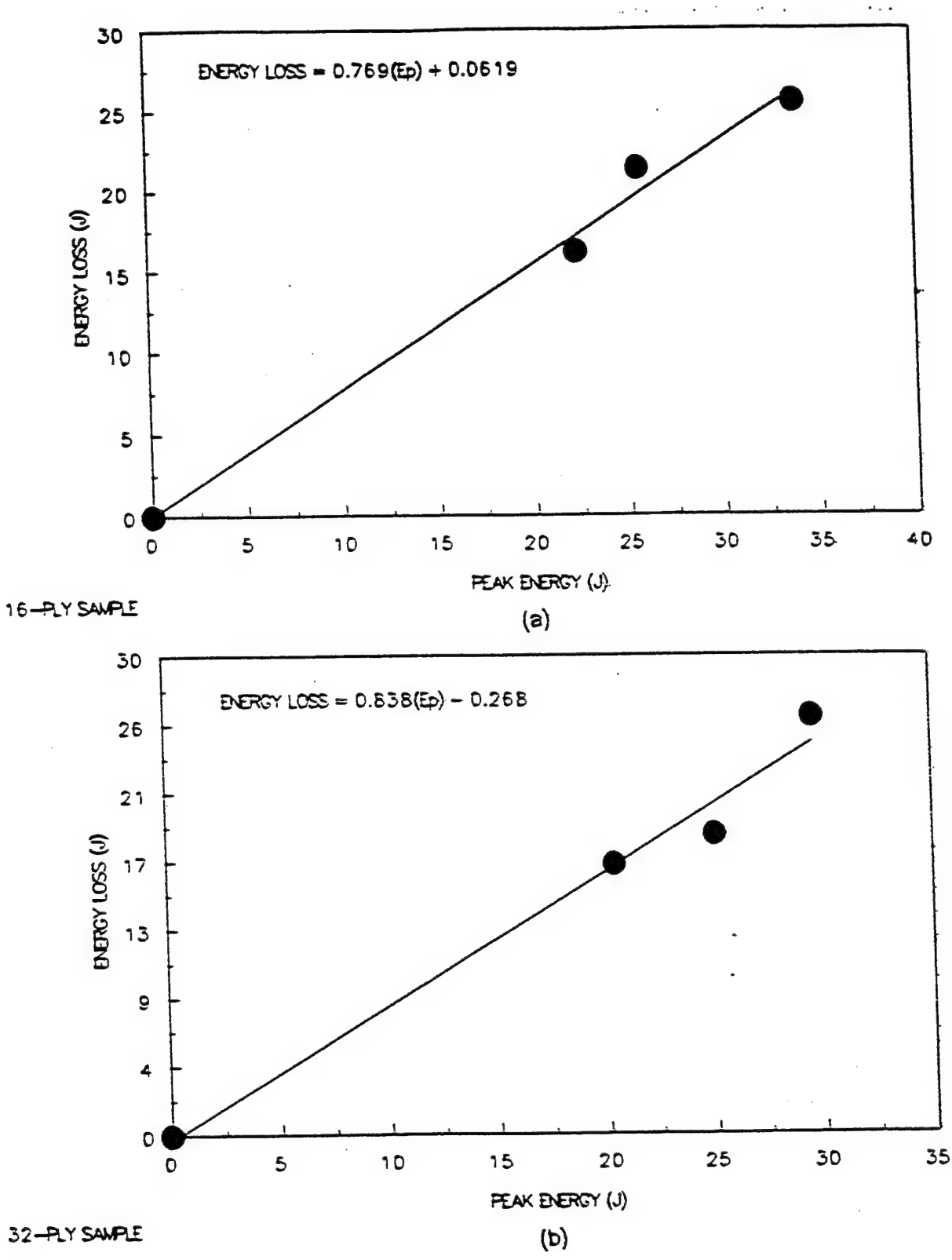

Figure 15. (a) Energy loss variation with absorbed energy for (a) 16-ply and (b) 32-ply graphite/epoxy laminates.

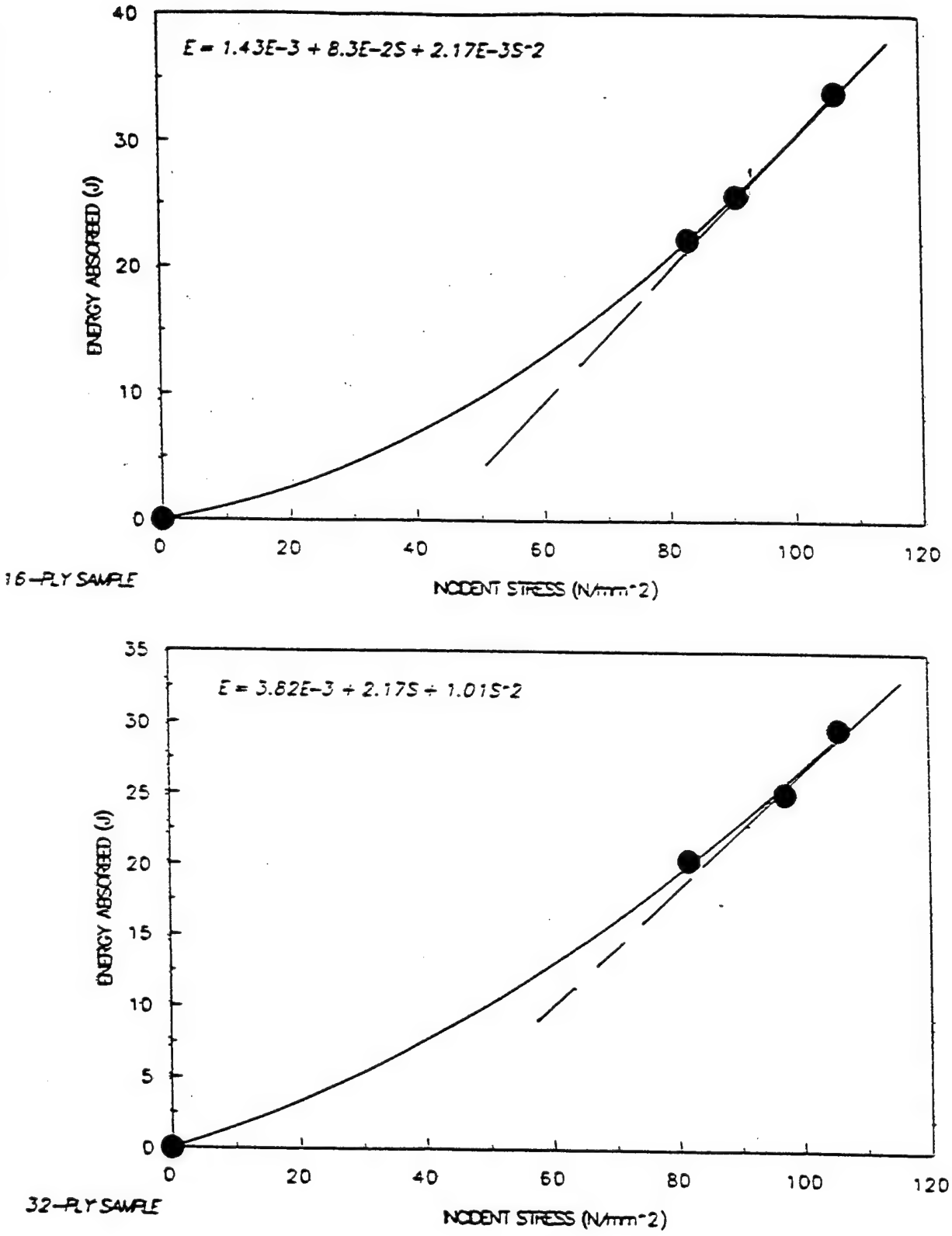

Figure 16 (a). Variation of energy absorption with maximum incident stress level for (a) 16-ply and (b) 32-ply graphite/epoxy laminates.

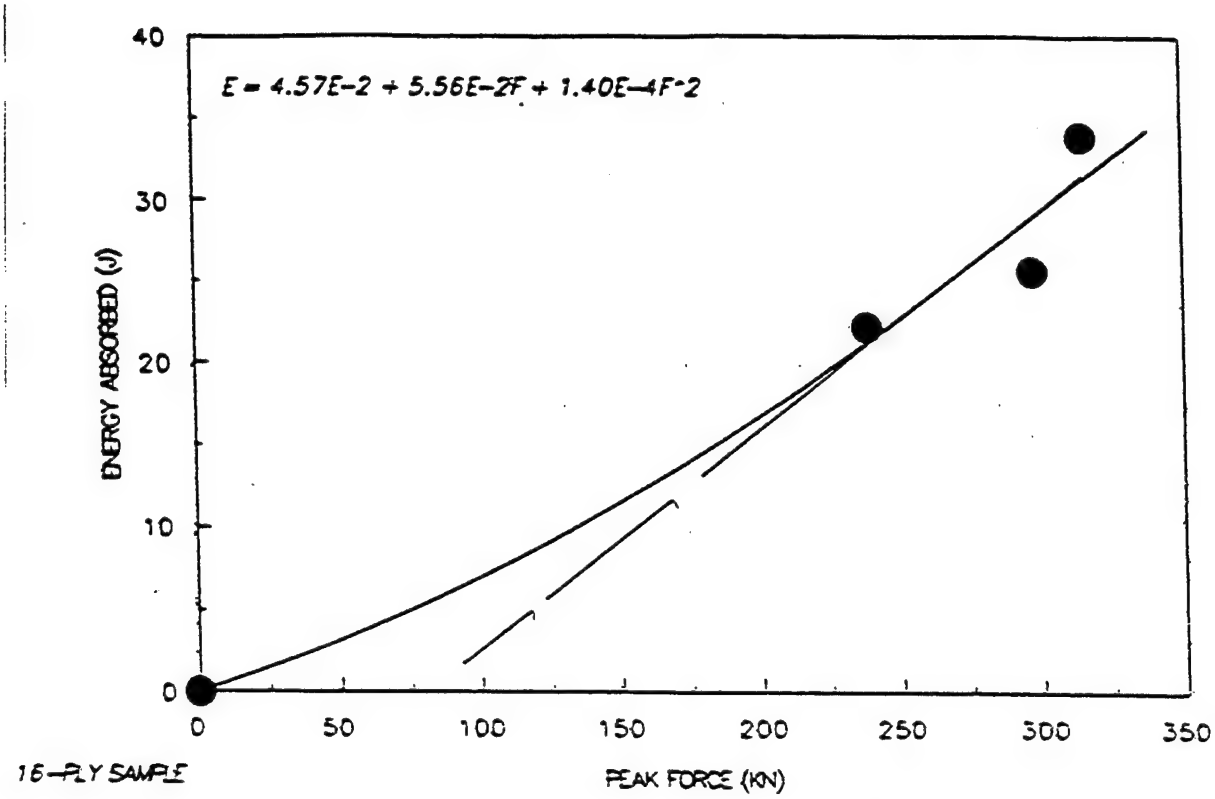

16-PLY SAMPLE

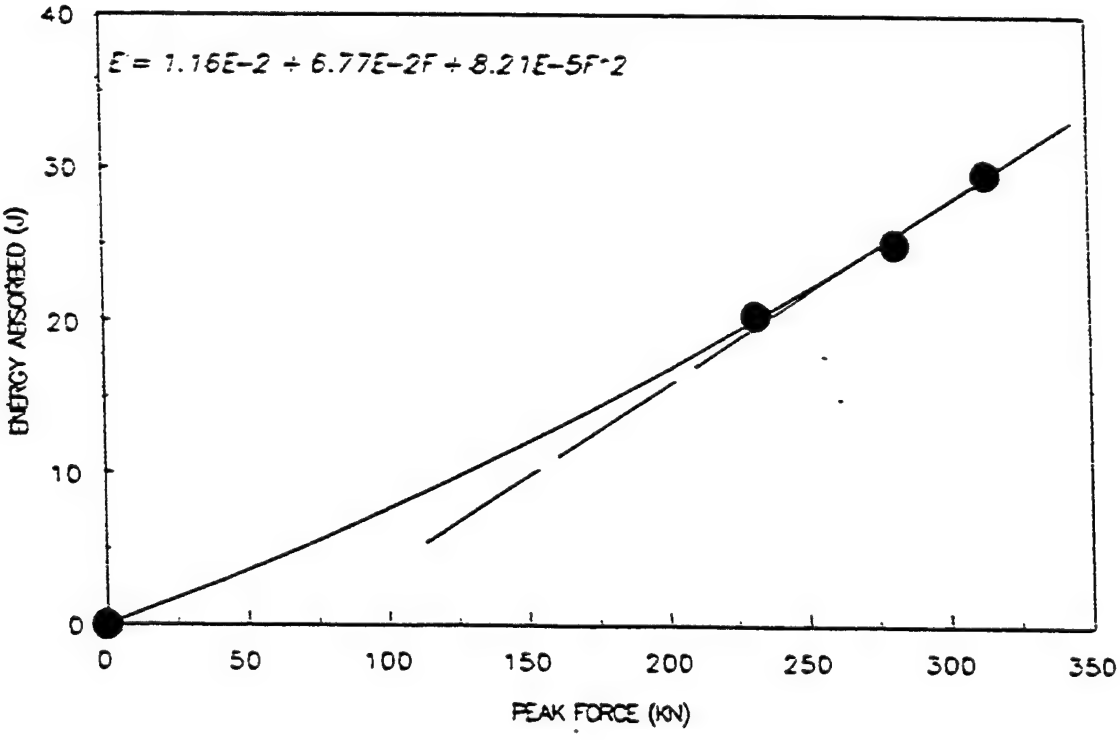

32-PLY SAMPLE

Figure 16 (b). Variation of energy absorption with peak force for (a) 16-ply and (b) 32-ply graphite/epoxy laminates.

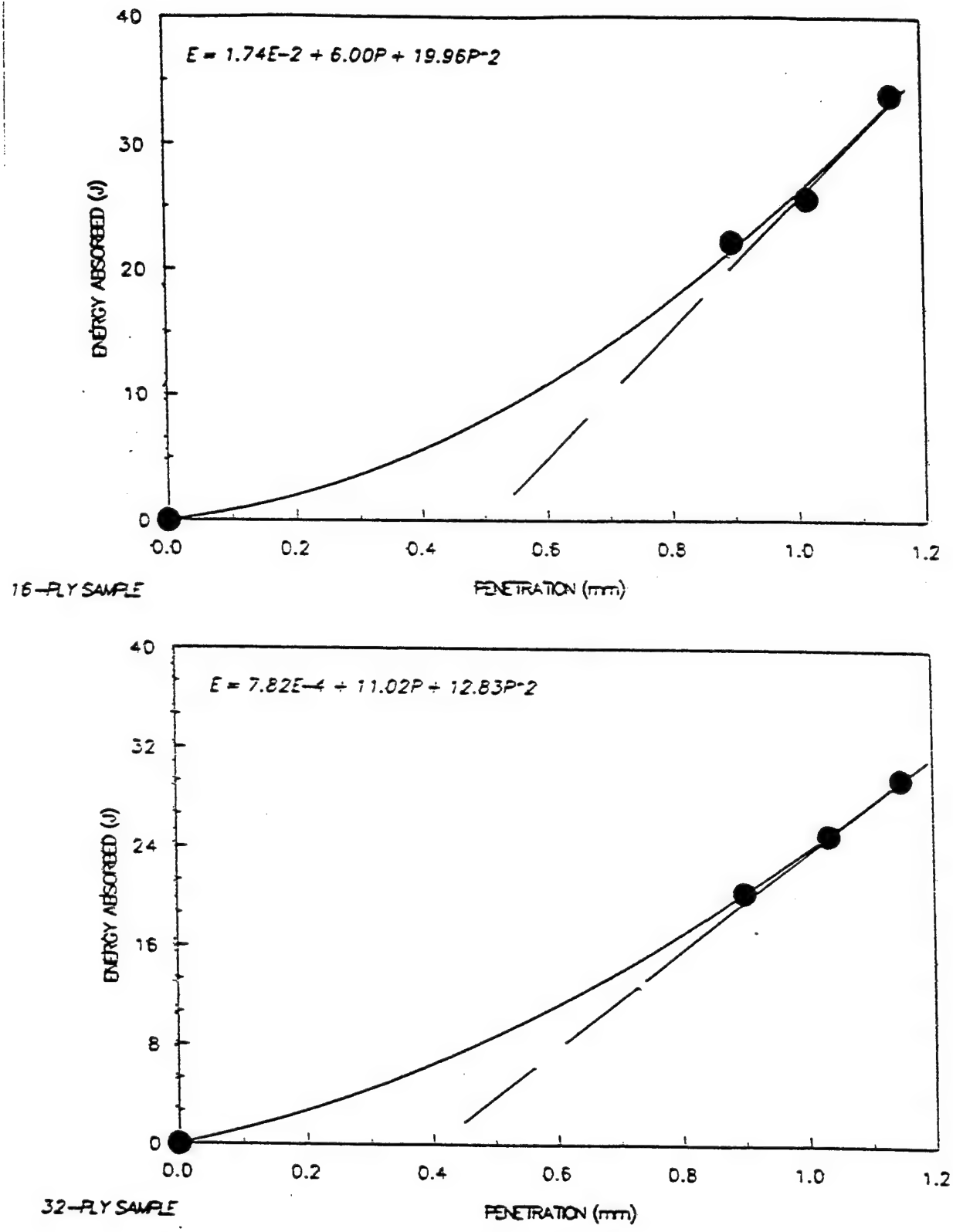

Figure 16 (c). Variation of energy absorption with penetration for (a) 16-ply and (b) 32-ply graphite/epoxy laminates.

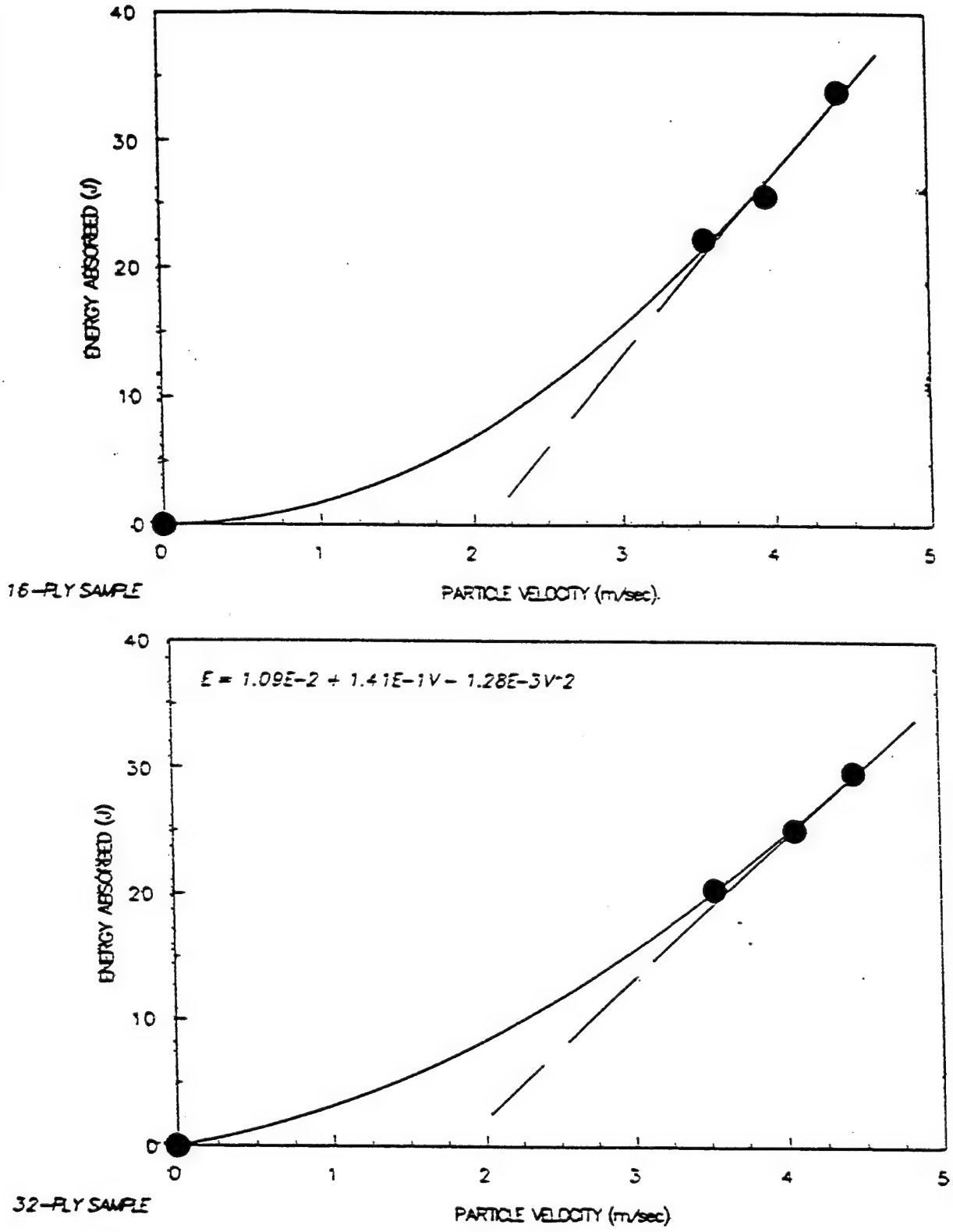

Figure 16 (d). Variation of energy absorption with particle velocity for (a) 16-ply and (b) 32-ply graphite/epoxy laminates.

response region. This energy conservation can also be seen in Figures 16 (a-d) which seems to demonstrate that the damage process is not a linear function of the impact energy for all stages of the damage process. Further investigation and data are needed to verify this. The important difference between these results is that perforation was achieved on the 8- and 16-ply specimens for all impact energies, but no perforation occurred on the 32-ply samples at these energies. The analysis neglects the effect of the indentor's conical shape and changes in contact area with penetration. As the indentor penetrates, its contact area increases. This is not true with the 32-ply specimen because there was no penetration for impact energy used for Figure 16. The indentor is currently being modified with a longer uniform protruding nose to avoid the anomaly of having the contact area increase with penetration.

5.8 Delamination Threshold and Damage Propagation Energy

A delamination threshold kinetic exit for graphite/epoxy and crack propagation along the fiber direction increases with impact energy. As further characterization of the damage process, the height (h), delamination damage length at the rear surface (L_d), and entrance width (w) of 16-ply specimen, under different impact energies and same fiber lay-up, were measured and their ratio plotted against energy absorbed in Figure 17(a). The variation or progression of length (along the diameter) of the damaged area with impact energy is shown in Figure 17(b) and the associated photographs in Figure 26. The result shows that the damage length or area propagates linearly with impact energy as

$$L_d = GV_I + G_o. \tag{27}$$

where 1/G is a measure of the rate of crack propagation and G_0 is a constant. Earlier investigators (The et al. 1993) observed the same phenomena via C-scan and demonstrated a threshold impact velocity above which cracks will begin to propagate. This threshold velocity was obtained by extrapolating the line to a zero-damage width and determining the velocity value. From Figure 17(b), the threshold velocity (striker velocity) for initiation of cracks in a 16-ply specimen is 13.5 m/s. The threshold impact energy for initiation of a visible crack on the rear surface of 16-ply specimens is 106 J. Given an impact velocity of 13.1 m/s and using equation 5(b), the difference between the experimental and predicted values remains less than 4%. Since the rear surface crack is initiated before perforation is achieved, the critical velocity for crack initiation may be less than the ballistic velocity. An extension of the analysis to determine ballistic limit velocity based on experimental and energy models will be included in the final report. An experimental estimate of the ballistic limit energy is in Figure 17. The present analysis however,

shows clearly that a threshold kinetic energy exists above which crack initiation on the rear surface will be visible. The crack length and size increase with impact energy. Examination of the damage pattern shows that the periphery of the hole's entrance side was smooth while fibers were still attached to the rear side. For complete penetration or perforation, the damage pattern on the rear side forms a flat top conical structure of height, *h*. Although more experimental points are needed near the ballistic point region, Figure 17(a), shows perforation is expected for impact velocities above 13.1 m/s and the crack propagates linearly from that point according to equation 27. This result collaborates with Figure 17(b) and shows a definite trend towards critical velocity. Further investigation is needed at very small increments of impact energy to determine the abrupt drop near this critical region.

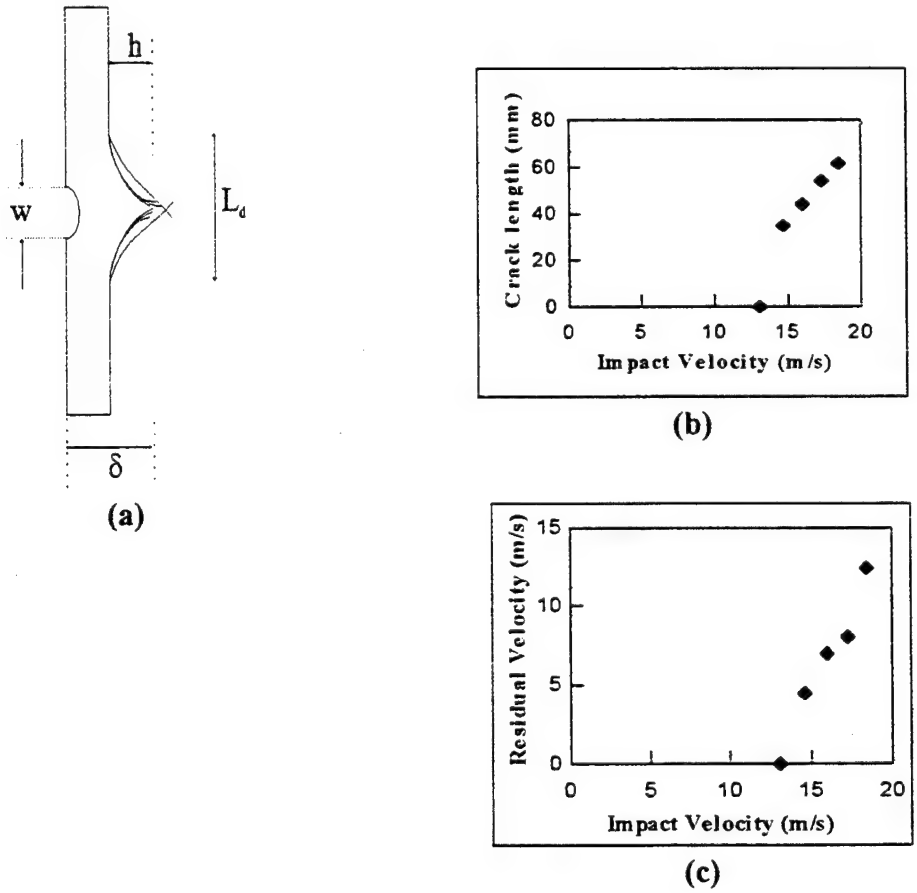

Figure 17. (a) Schematic of perforated laminated plate, (b) variation of surface crack length with impact velocity, and (c) residual velocity vs impact velocity for 16-ply graphite/epoxy.

5.9 Effect of Fiber Lay-Up on Surface Damage and Delamination

Figures 18-21 compare the effect of fiber orientation on the nature of damage. GP1 has a stacking sequence of $[\pm 45]_{2s}$ while GP2 has a sequence of $[45/0/90]_s$ and the same thickness (0.25 mm) and cross sectional area. GP3 and GP4 have sequences of $[45/0/90]_{2s}$ and $[45/0/90]_{4s}$ respectively. The energy absorption curve for GP2 is less than that of GP1. The figure also indicates a decreasing energy during the equilibrium (constant velocity) stage for the GP2 laminate and larger amplitude of the force reversal in GP2. These two observations indicate that greater internal damage and residual energy are possible for the GP2 laminate than for GP1. Although the particle velocity appears to be independent of the fiber lay-up, Figure 21(b) shows some vibration and ringing for the GP1 specimen. It appears that GP1 is experiencing a higher sample stress factor and more energy absorption in the damage process than GP2. This is further revealed in the photographs of Figure 21 and shows that the major damage event for the GP2 laminate is fiber push out and delamination which starts much earlier than in GP1 as shown by the early decrease in energy in Figure 20 (a).

Figure 21 (a & b) displays the rear exit surface of the plate and shows fact that the damage pattern is consistent with failure in the fiber direction for the GP2. Since previous studies show that delamination increases from rear surface to the contact point, it appears that GP2 has a tendency to split in the middle. The GP1 failure pattern, on the other hand, appears to involve a tensile fracture which is transverse to the direction of the fiber and appears to grow obliquely to the interface (Figure 21 b). Although small delamination may be occurring, it appears that the major damage event in GP1 is matrix cracking and more localized fiber breakage which are expected to occur at lower energies than delamination. This observation is similar to that of other researchers [Sierakowki (1993)]. Internal crack studies by Dashin (1987) using SEM shows that in the absence of delamination, transverse cracks grow perpendicular to lamina interface but when delamination exist, it grows obliquely to the laminar interfaces. Thus, when subjected to identical energies the GP2 sample has a greater tendency to suffer more catastrophic failure than GP1. In all the cases investigated, GP2 suffered more catastrophic failure than GP1 (given identical impact conditions). Results also show that it is conceivable for transverse cracks and delamination to occur simultaneously depending on fiber lay-up and orientation.

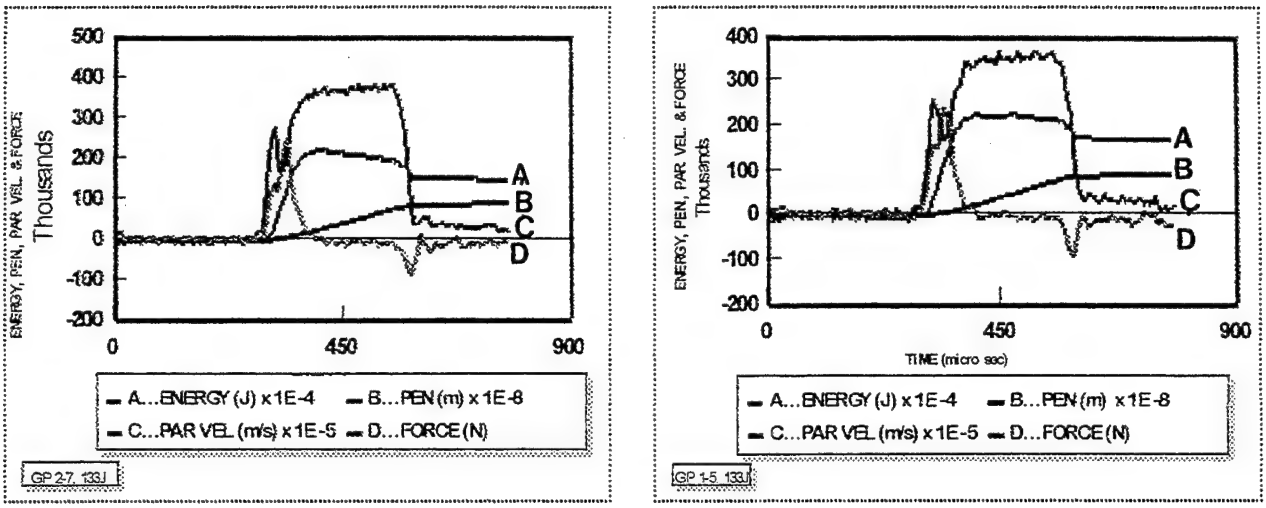

(a) (b)

Figure 18. Energy, Penetration, Particle velocity and force-time curve for (a) $[\pm 45/0/90]_s$ and (b) $[\pm 45]_{2s}$ fiber lay-up at 133 J striker impact energy. (Note: Energy (J) x 10^{-4}; Particle Velocity (m/s) x 10^{-5} ; and Penetration (meters) x 10^{-8})

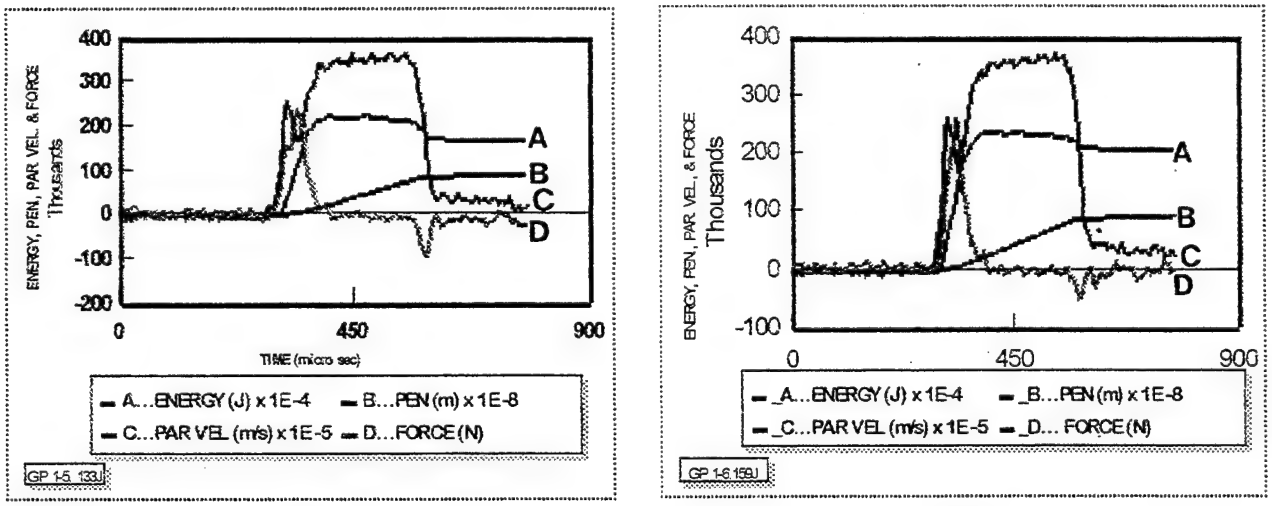

(a) (b)

Figure 19: Energy, Penetration, Particle velocity and force-time curve for (a) $[\pm 45/0/90]_s$ and (b) $[\pm 45]_{2s}$ fiber lay-up at 159 J striker impact energy. (Note: Energy (J) x 10^{-4}; Particle Velocity (m/s) x 10^{-5} ; and Penetration (meters) x 10^{-8})

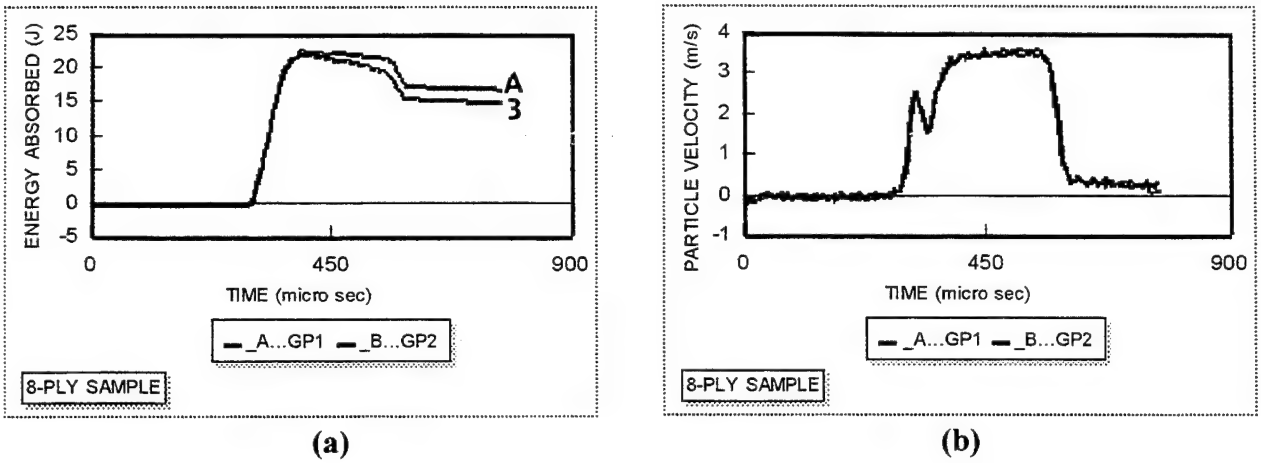

Figure 20. Variation of energy absorbed (a) and particle velocity (b) with fiber lay-up for 8-ply graphite/epoxy laminate for $[\pm 45]_{2s}$ (GP1) and $[\pm 45/0/90]_s$ (GP2) at 133 J striker impact energy.

5.10 Damage Initiation

Damage initiation depends on thickness and impact energy. Figures 22-26 show the results of experiments to investigate the threshold of crack initiation on the rear surface, perforation, and plug push-out for 16- and 32-ply samples. The 16-ply specimens (Figures 24 and 26) were penetrated at 106 J, 133 J, 159 J, 186 J, and 212 J striker impact energies, while the 32-ply specimens (Figures 23, 25, and 26) were penetrated at 133 J , 159 J, 186 J, 212 J, and 260 J (not shown in the Figure but in photograph) impact energies. The point of force reversal marks the total deformation of the laminate and the maximum area of perforation (contact area). The point of the maximum force and subsequent rapid drop is correlated with the onset of damage that begins with matrix cracking and leads to plug push out and delamination. Note that particle velocity and energy absorbed begin to attain a zero slope just after the initial compressive contact force drops to zero. This marks the beginning of a transition zone from one form of damage mechanism to another. It appears that at this zone, the compressive stress wave begins to reflect back as a tensile wave. Such reflection is the primary cause of mode I delamination. In the present investigation, the tension results from a reflecting stress wave. All force-displacement

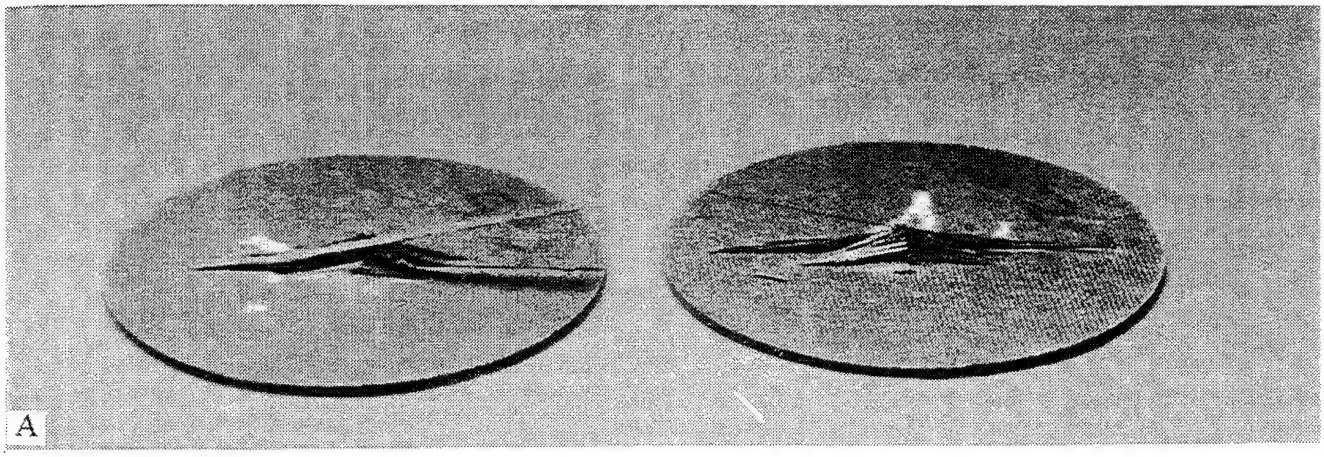

MATERIAL: GRAPHITE/EPOXY
FIBER LAY UP: $[\pm 45/0/90]_S$
PLATE THICKNESS: 1.042mm (0.041 in)
DENSITY: 1624.92 kg/m^3 (5.87 x 10^{-2} lb/in^3)
IMPACT ENERGY: 159 J (1.03 x 10^6 Pa)

MATERIAL: GRAPHITE/EPOXY
FIBER LAY UP: $[\pm 45/0/90]_S$
PLATE THICKNESS: 1.042mm (0.041 in)
DENSITY: 1624.92 kg/m^3 (5.87 x 10^{-2} lb/in^3)
IMPACT ENERGY: 133J (8.59 x 10^5 Pa)

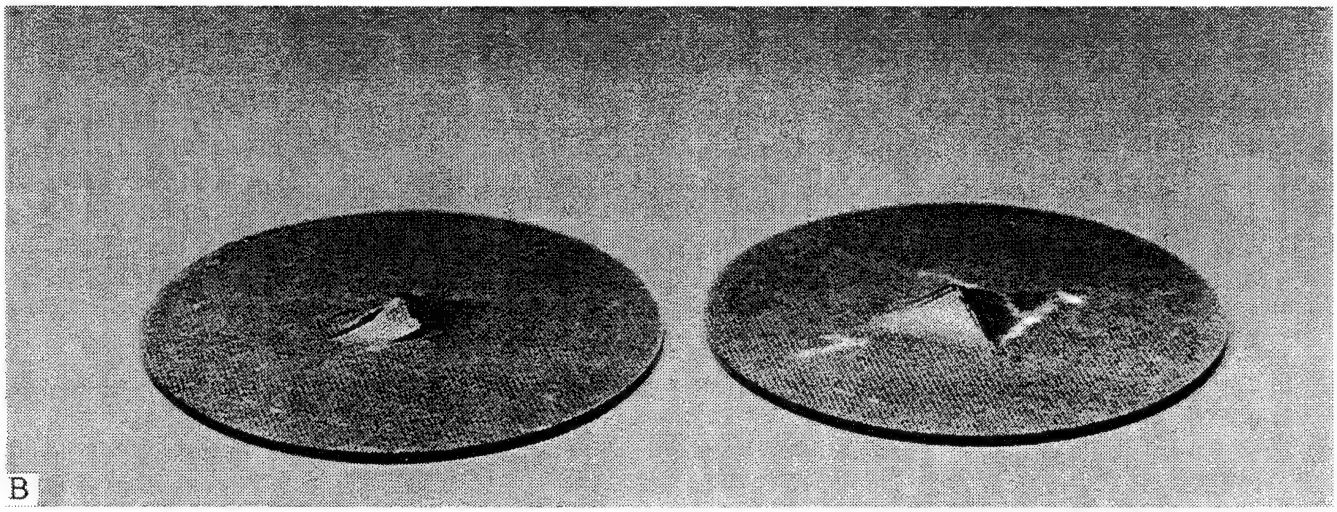

MATERIAL: GRAPHITE/EPOXY
FIBER LAY UP: $[\pm 45]_{2S}$
PLATE THICKNESS: 1.042mm (0.041 in)
DENSITY: 1624.92 kg/m^3 (5.87 x 10^{-2} lb/in^3)
IMPACT ENERGY: 133 J (8.59 x 10^5 Pa)

MATERIAL: GRAPHITE/EPOXY
FIBER LAY UP: $[\pm 45]_{2S}$
PLATE THICKNESS: 1.042mm (0.041 in)
DENSITY: 1624.92 kg/m^3 (5.87 x 10^{-2} lb/in^3)
IMPACT ENERGY: 159 J (1.03 x 10^6 Pa)

Figure 21. Photographs of damaged graphite/epoxy laminates showing the damage pattern for (a) $[\pm 45/0/90]_s$ and (b) $[\pm 45]_{2s}$ and varying impact energies (133 J and 159 J)

curves show that the amplitude of the force reversal depends on orientation, sample thickness, and initial compressive load.

Incipient delamination for the 32-ply sample occurs when the impact energy is above 233 J as clearly indicated by the vibration in Figure 22 (a). Note that the major change in the amplitude of the force release occurs at 233 J (Figure 22 (b) and Figure 23 (b)). The presence of the tensile wave shows that some stable damage is occurring in the laminate before a major event above 233 J (Figure 23 (a)). With the exception of the abrupt increase at 159 J in Figure 22 (a) (which could be an experimental or statistical uncertainty), the peak force appears to be constant until this major event in the neighborhood of threshold kinetic energy for perforation. Studies have shown that failure of brittle materials such as graphite/epoxy is initiated at the penetration of the contact area and governed by the material's tensile strength [Zukas el al. 1992]. The comparison of absorbed energy with time (Figure 24) shows that the 32-ply samples absorb slightly more energy than 16-ply samples. The energy absorbed by the penetration event is not linear and may exhibit an energy region between perforation and penetration threshold. Although such region is not very clear in this result, the result leads to a quantitative search for such transition energy region.

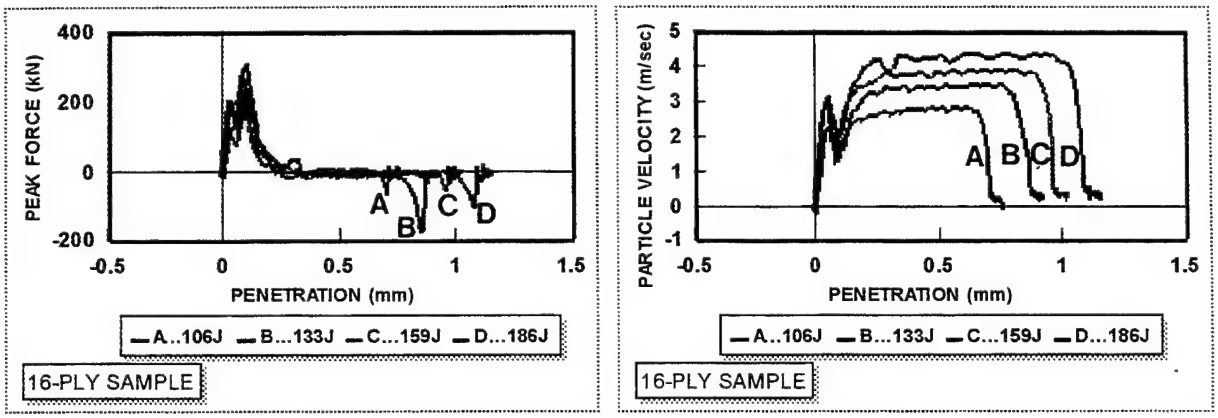

(a) (b)

Figure 22. (a) Force-displacement and (b) particle velocity-displacement at varying impact energies of the striker for damage initiation study of 16-ply graphite/epoxy laminates.

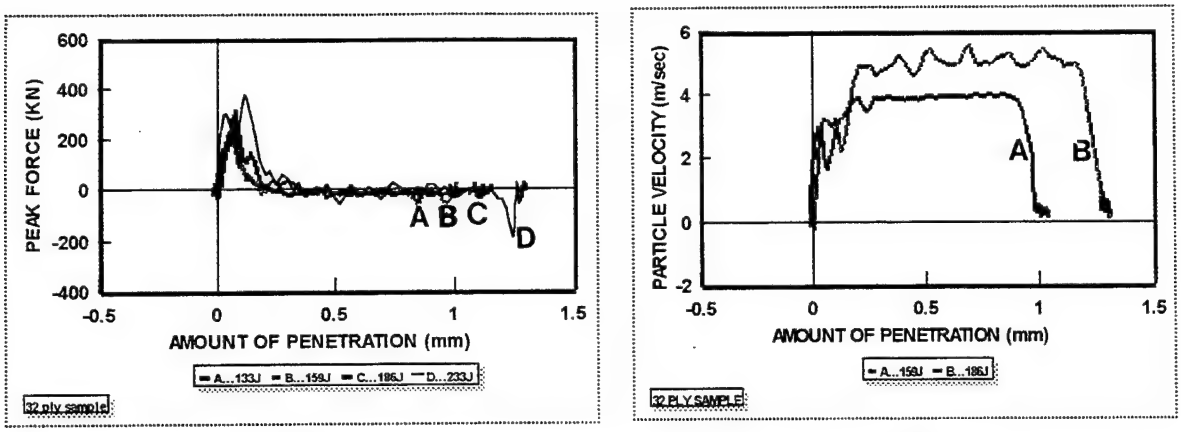

(a) (b)

Figure 23. (a) Force-displacement and (b) particle velocity-displacement at varying impact energies of the striker for damage initiation study of 32-ply graphite/epoxy laminates.

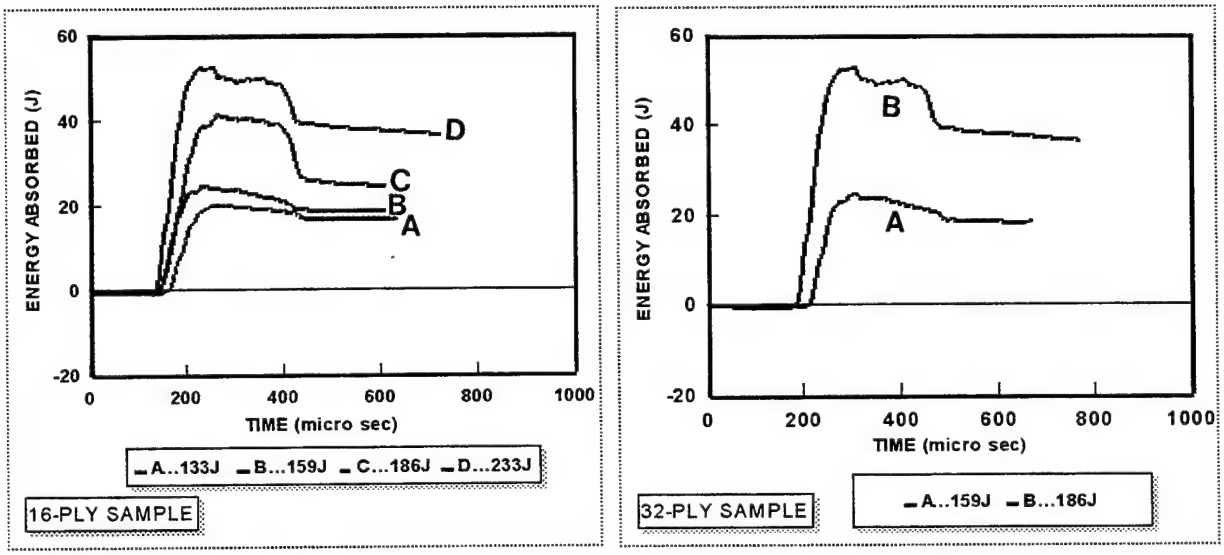

(a) (b)

Figure 24. Variation of absorbed energy with impact energy for (a) 16-ply and (b) 32-ply graphite/epoxy laminates at varying impact energies of the striker.

5.11 Plugging and Delamination

Plugging and Delamination of 16-ply specimens occur at 186 J and 260 J for the 32-ply. The photographs in Figures 25 and 26 clearly show a difference in the level of damage, and reveal that the major event is plug push out and delamination. The figures show entrance and exit side damage effects of the laminate and demonstrate showing matrix cracking, buckling, and fiber breakage. For the 16-ply laminate, a rear surface crack became visible at 106 J (not shown) and propagated as the energy increased to perforation at 159 J. Notice the lateral damage propagation and punch-through perforation at the 212 J impact energy. Although it is not noticeable in the figure, a rear surface crack on the 32-ply laminate was first observed at 233 J. The crack propagated as the energy increased until a complete plug push-out and failure occurred. The critical energy for perforation is about 159 J (10 J/ply) for the 16-ply specimen. The perforation result for a 32-ply was inclusive, however, there was plug push-out at 260 J. It appears from the visible nature of the damage that the impact energies of 212 J and 260 J may have exceeded the ballistic limit energy of these specimen and may also have been affected by changes in the contact area. A difference of 27 J (233 J to 260 J) of energy, in the case 32-ply specimens, caused a major difference in the propagation of the damage around the ballistic limit region. This shows the very critical nature of this region and the necessity of further investigation. Table 2 below summaries the results. The results are also collaborated with previous results from Figure 17 which establishes the threshold velocity in the neighborhood of 13.5 m/s (113 J) .

Table 2. Damage initiation energy (J)/ply in graphite/epoxy

Specimen	Crack Initiation	Perforation	Plug Push-out
16-ply	106 J	159 J	212 J
32-ply	233 J	Not Determined	260 J
Energy (J)/ply	**7 ± 1**	**10**	**11 ± 3**

Energy (J)=1.06 impact stress (psi).

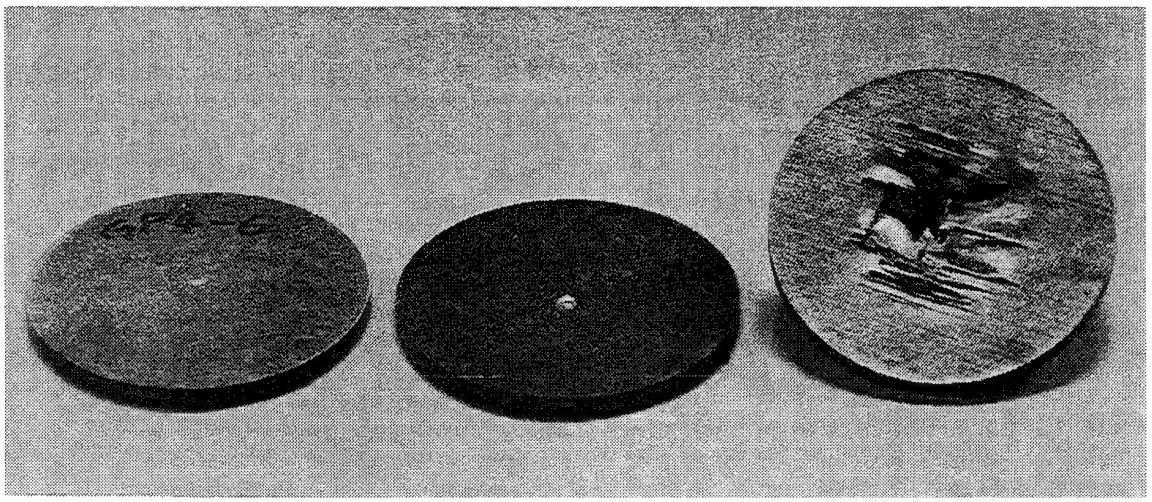

A

MATERIAL: GRAPHITE/EPOXY	**MATERIAL:** GRAPHITE/EPOXY	**MATERIAL:** GRAPHITE/EPOXY
FIBER LAY UP: $[\pm 45/0/90]_{4S}$	**FIBER LAY UP:** $[\pm 45/0/90]_{4S}$	**FIBER LAY UP:** $[\pm 45/0/90]_{4S}$
PLATE THICKNESS: 4.064mm (0.160 in)	**PLATE THICKNESS:** 4.064mm (0.160 in)	**PLATE THICKNESS:** 4.064mm (0.160 in)
DENSITY: 1624.92 kg/m^3 (5.87 x 10^{-2}lb/in^3)	**DENSITY:** 1624.92 kg/m^3 (5.87 x 10^{-2}lb/in^3)	**DENSITY:** 1624.92 kg/m^3 (5.87 x 10^{-2}lb/in^3)
IMPACT ENERGY: 159 J (1.03 x 10^6 Pa)	**IMPACT ENERGY:** 233 J (1.50 x 10^6 Pa)	**IMPACT ENERGY:** 260 J (1.68 x 10^6 Pa)

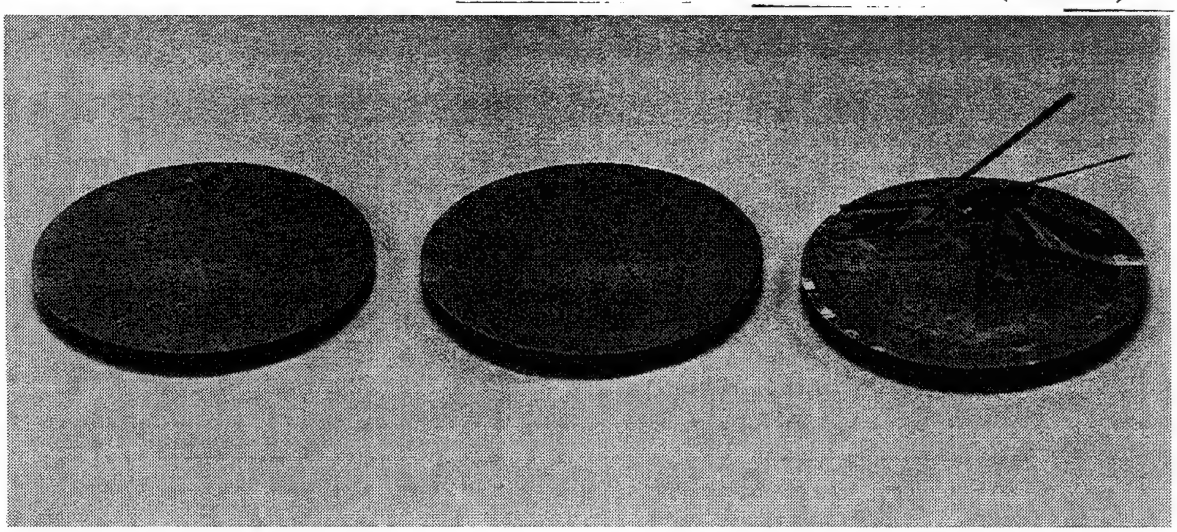

B

Figure 25. Photographs of damaged graphite/epoxy laminates showing the damage pattern for 32-ply (a) entrance surface damage (b) rear surface damage for varying impact energies (159 J, 233 J and 260 J).

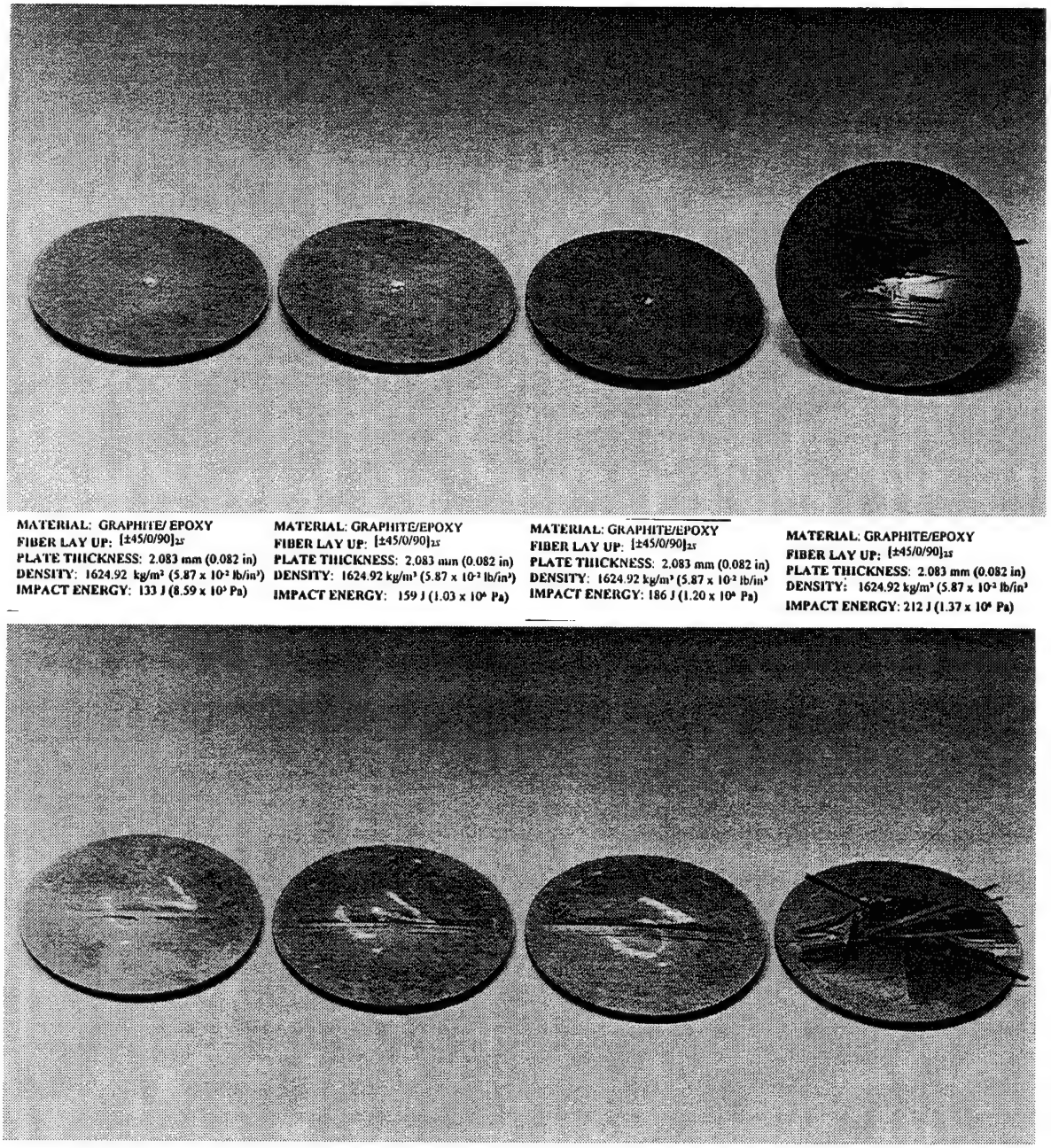

Figure 26. Photographs of damaged graphite/epoxy laminates showing the damage pattern for 16-ply (a) entrance surface damage and (b) rear surface damage for varying impact energies (133 J, 159 J, 186 J, and 212 J).

5.12 Validity of the Perforation Experiments

The results of preliminary studies (Sivapuram et al. 1994) conducted at CRREL are displayed in Figures 27 and 28. The similarity of CRREL and Dillard results, although using different approaches of experimentation and data analysis, serve to verify the validity of the techniques, the functionality of the apparatus, and the precision of the results. The CRREL test samples are 30-ply $[\pm 45/0_2/90_2]_3$, laminates of graphite/epoxy impacted at 80 psi and 100 psi impact stress. The double reflection is noticeable, but is so small that it did not appear in the force curve. The results (Figure 28) indicate that the higher the impact energy (stress), the greater the damage on the laminate with fiber pull-out and greater delamination as shown in Figure 28 (b).

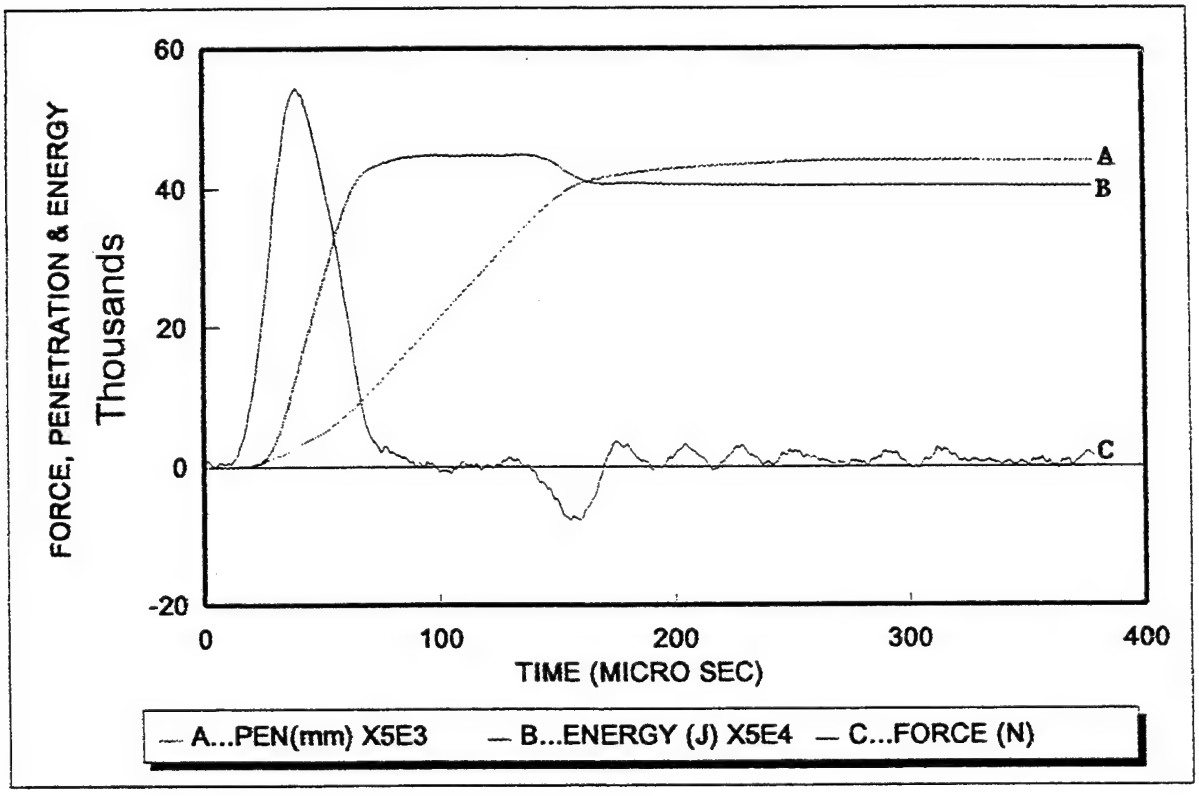

Figure 27. Variation of impact force and energy absorbed for experiments performed at CRREL.

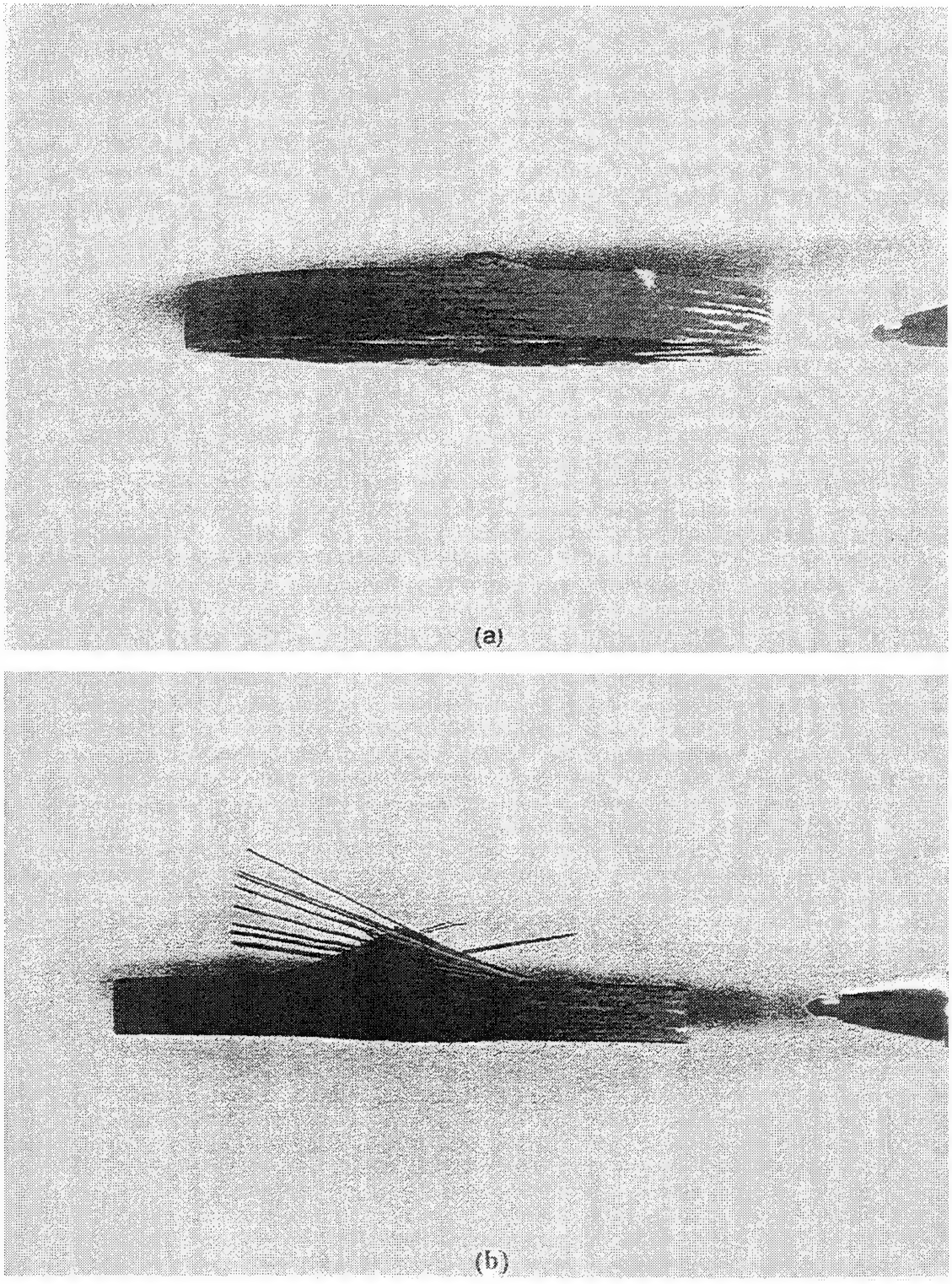

Figure 28. Photographs of damaged 30-ply graphite/epoxy laminates for experiment performed at CRREL at (a) 80 psi and (b) 100 psi.

6. CONCLUSIONS

1. The Dillard University High Energy Impact Research Laboratory (HEIRL) has been successfully established for perforation and wave propagation studies of composite materials. A Hopkinson bar, with appropriate modifications, has been applied towards perforation studies of graphite/epoxy laminates.

2. A threshold energy exists below which a crack will not form and propagate. The threshold kinetic energy per laminate needed for damage initiation in unidirectional graphite/epoxy laminate is 7 ± 1 J/ply for crack initiation at the rear surface, 10 J/ply for perforation and 11 ± 3 J/ply for plug push out. Analysis to separate perforation threshold from that of push out needs more examination to improve the accuracy and precision of the measurements.

3. Incipient damage is revealed by increased force reflection (greater amplitude of the force reversal). Crack formation propagates linearly with impact energy. For 16-ply laminates, the striker threshold impact velocity to initiate damage is 13.5 m/s corresponding to 113 J impact energy.

4. Incident stress is proportional to striker impact energy but independent of plate thickness. The particle velocity and loading force on the specimen linearly depend on the incident stress. The energy transferred to the specimen in the damage process increases with increase in incident stress.

5. High oscillations are observed in the particle velocity curve at high stress levels and indicates greater specimen damage. Although stress waveforms, particle velocity, and force do not vary with laminate thickness for the same impact energy, the energy absorbed is thickness dependent. The thicker the plate, the greater the energy lost by the indentor (absorbed by the plate).

6. The relationship between energy absorbed, particle velocity, impact velocity, and penetration during the first damage stage (assumed to be matrix cracking and fiber breakage) appear quadratic. The relationship appear to change to linear as a critical particle velocity and impact energy is attained. As a first-order approximation, the onset of delamination is identified at the impact energy corresponding to a major increase in the reflected force amplitude and the point of deviation from linearity (see Figure 16).

7. Fiber lay-up has very strong effect on the nature of damage. The damage pattern sustained by the $[\pm 45]_{2s}$ lay-up is localized in the transverse direction and oblique to the interface while damage pattern for the $[\pm 45/0/90]_s$ lay-up is the direction of the fiber as an indication of delamination due to tensile stress wave. From a design view point, $[\pm 45]_{2s}$ will suffer less catastrophic damage than the $[\pm 45/0/90]_s$ lay-up at the same impact energy.

8. The multiple reflections observed in this study is mainly an anomaly caused by reflections at the interfaces due to impedance mis-match at the incident bar/indentor interface and indentor/specimen interface.

9. The agreement between research performed at Dillard's High Energy Impact Research Laboratory (HEIRL) and that at the Cold Region Research and Engineering Laboratory (CRREL) establishes the validity of procedures and results presented here.

7. CONTINUING RESEARCH

1. Further research (involving deply and SEM analysis of the perforated samples) is being performed at the University of New Orleans to characterize the failure mode. C-scan evaluations of the laminates will be performed to establish the areas of damage and the extent of delamination from the rear surface of laminate.

2. Different physical models namely, impulse momentum, energy-balance, quasi-static Hertzian contact, and a combination of the above are being applied to predict the ballistic limit energy.

3. Further investigation is needed to determine if damage mechanism contributes to double-peak phenomenon in the perforation of composite plate.

4. Use of appropriate methods to determine the interactions between the parameters investigated in this report.

5. Appropriate scaling theory is being investigated for determination of the region of damage mechanism.

Acknowledgment
This project is funded by the Flight Dynamics Directorate, Wright-Patterson Air Force Base under contract #F33615-93-C-3411. Mr. Greg Czarnecki served as the Project Monitor. Work is performed at Dillard's newly established High Energy Impact Research Laboratory.

REFERENCES

1. Agarwal, B. D. and Brouyman, LJ (1979), "Analysis and Performance of Fiber Composites" John Wiley and Sons, New York
2. Bickle, LW (1970), "An Introduction of the Use of Strain Gages for the Measurement of Propagating Strain Wave", Sandia Laboratories, Albuquerque, Mew Mexico.
3. Czarnecki, Greg (1991), " A Preliminary Investigation of Dual Mode Fracture Sustained in Graphite /epoxy Impacted by High Velocity Spherical Projectile" , MS. Thesis, University of Dayton, Ohio
4. Daniel, I. M., and Wooh, S. C. (1990). " Deformation and Damage of Composite Laminates Under Impact Loading," Impact Response and Elastodynamics of Composite, ed by A. K. Mal and Y.D.S. Rajapakse, AMD-volume 116, Winter Annual Meeting, Nov. 25-30, pp. 11-26.
5. Dutta, P.K, Dannis, F, and Kalafut, J (1987), " The CREEL Hopkinson Bar Apparatus", Special Report 87-24.
6. Dutta, P.K., Hui, D. and Altamirano, M.R. (1991), "Energy Absorption of Graphite/Epoxy Plates under Hopkinson Bar Impact", CRREL Report 91-20, October.
7. Dutta, P.K. "The Determination of Stress Waveforms produced by Percussive Drill Pistons of various geometric Design (1968)", Rock Mechanics. Min Sci. Vol. 5, P. 501-518.
8. Graaff, Karl. (1975). " Wave Motion in Elastic Solids", Ohio State University Press
9. Kim, KS (1985, "Dynamic Fracture under Normal impact loading of Crack Faces J. of Applied Mechanics, Vol, 52, pp. 585.
10. Kolsky, H (1953). Stress Waves in Solids, Oxford: Clarendon Press.
11. Nwosu, S. N, Dutta, P. K, and Hui, D (1994). "Stress Wave Propagation in Rocks and Unconsolidated Soil Samples by Vertical Dynamic Hopkinson Bar, "Proceedings of International Conference on Composites Engineering in New Orleans August 28-31, pp. 373-374.
12. Nwosu, S. N, Dutta, P. K, and David Hui (1994). "Characterization of Composite Materials by Vertical Dynamic Hopkinson Bar, "Proceedings of the 1994 Engineering Systems Design and Analysis Conference, July 4-7, in London PD-Vol. 64-2.
13. Nwosu, SN, Sivapuram S.K,, P.K. Dutta and David Hui (1994). "Graphite Epoxy Laminate Penetration at Low Temperatures, "Proceedings of International Conference on Composites Engineering in New Orleans August 28-31, pp. 137-138.
14. Ravichandran, G and Subbash, G (1994), "Critical Appraisal of Limiting Strain Rates for Compression Testing of Ceramics in a Split Hopkinson Pressure Bar", Journal of American Ceramic Society, Vol 77 January pp. 263-267
15. Shivakumar, E. W, and Illg, W (1985), "Prediction of Impact Force and Duration Due to Low Velocity Impact on Circular Composite Laminate", Transaction of ASME, Vol. 52, pp. 674.
16. Sivapuram S.K, S.N. Nwosu, P.K. Dutta and David Hui (1994). "Graphite Epoxy Laminate Penetration at Low Temperatures, "Proceedings of International Conference on Composites Engineering in New Orleans August 28-31, pp. 137-138.
17. Sjoblom, PO, Hartness, T, and Cordell,T (1988)." On Low velocity Impact testing of

composite materials", Journal of Composite Materials, Vol. 22, pp. 30-51.
18. Sun, C. T and Potti, S. V (1993) "High Velocity Impact and Penetration of Composite laminates", Proceedings of 9th ICCM Conference, P. 261-268.
19. Sun, C. T and Potti, S. V (1995), " Modeling Dynamic Penetration of Thick Section Composites", Proceedings of 9th ICCM Conference,
20. The, K. T, Morton, J, Souz J, and Baird, DG (1993) "Impact Damage Studies in AS4/PEEK and PEKK/HX1000", Proceedings of 9 th ICCM p 475-581.
21. Tan, TM, Sun, CT (1985) , "Use of Statistical Indentation Law in Impact Analysis of laminated Composite Plates", Transaction of ASME Vol. 52 , pp. 6-12.
22. Wu, H. T and George S. Springer (1988), " Impact Induced Stress, Strains, and Delamination in Composite Plates", Journal of Composite Materials, Vol. 22, pp 533.
23. Wu, E, Sheen, H. J, Chen, YC, and Chang, LC (1994), " Penetration Force measurement of Thin Plates by Laser Doppler Anemometry", Experimental Mechanics, June 1994, pp. 93-99.
24. Zhu, Guoqi, Goldsmith, W, and Dharan, C.K.H (1992), " Penetration of Laminated Kevlar by Projectiles-II. Analytical Model." Int. J. Solid Structures Vol 29, No. 4. Pp 421-436.
25. Zukas, JA, Nicholas, T, Swift, H, Greszczuk, LB, and Curran, D (1992), Impact Dynamics, Kreiger Publishing Co.

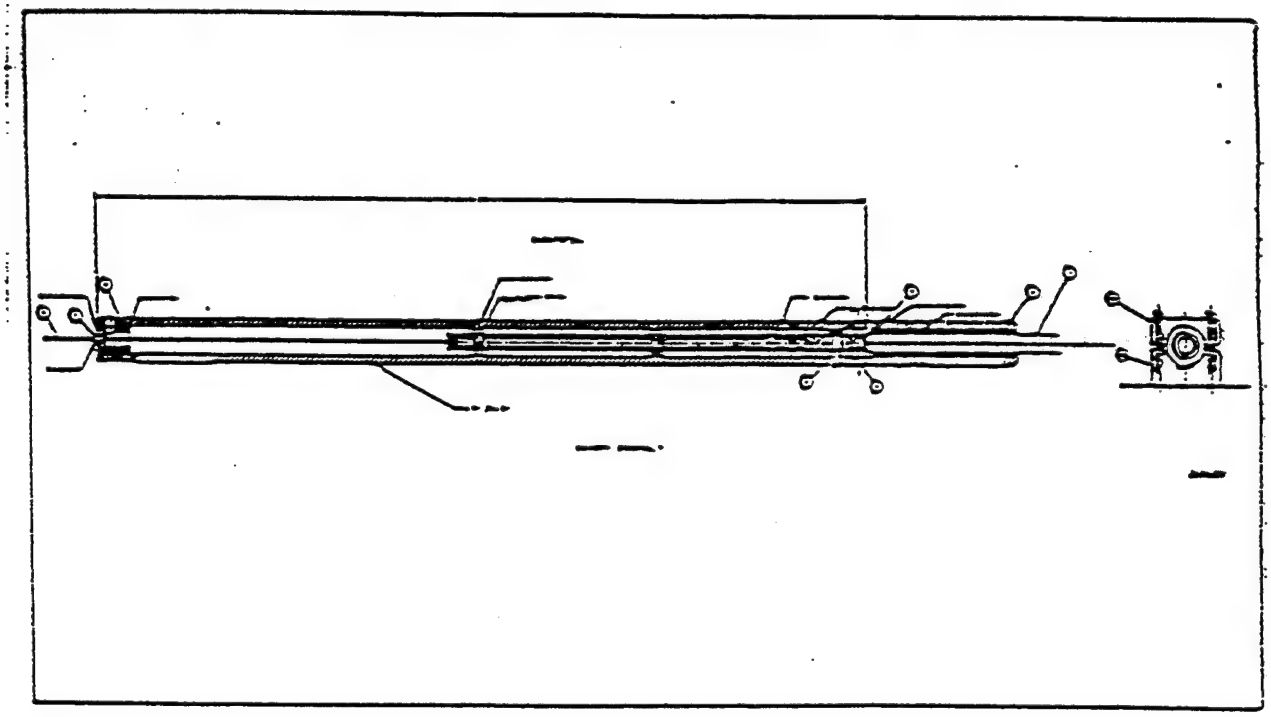

Design Layout of the Launch Cylinder

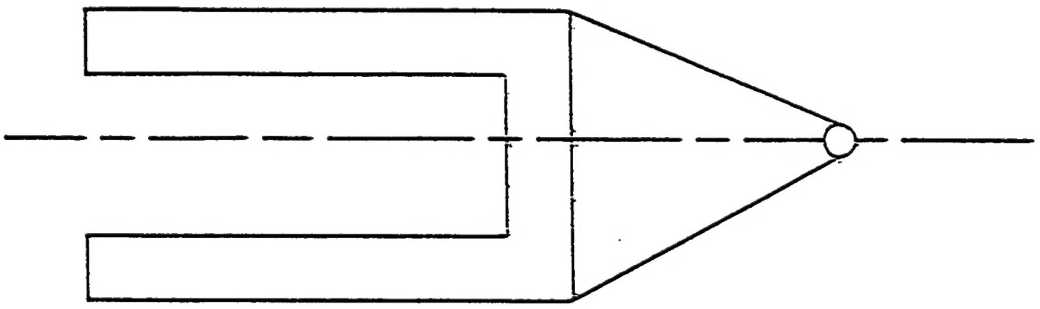

IMPACTOR FOR THE HOPKINSON BAR

HOPKINSON SET-UP IN THE ROOM

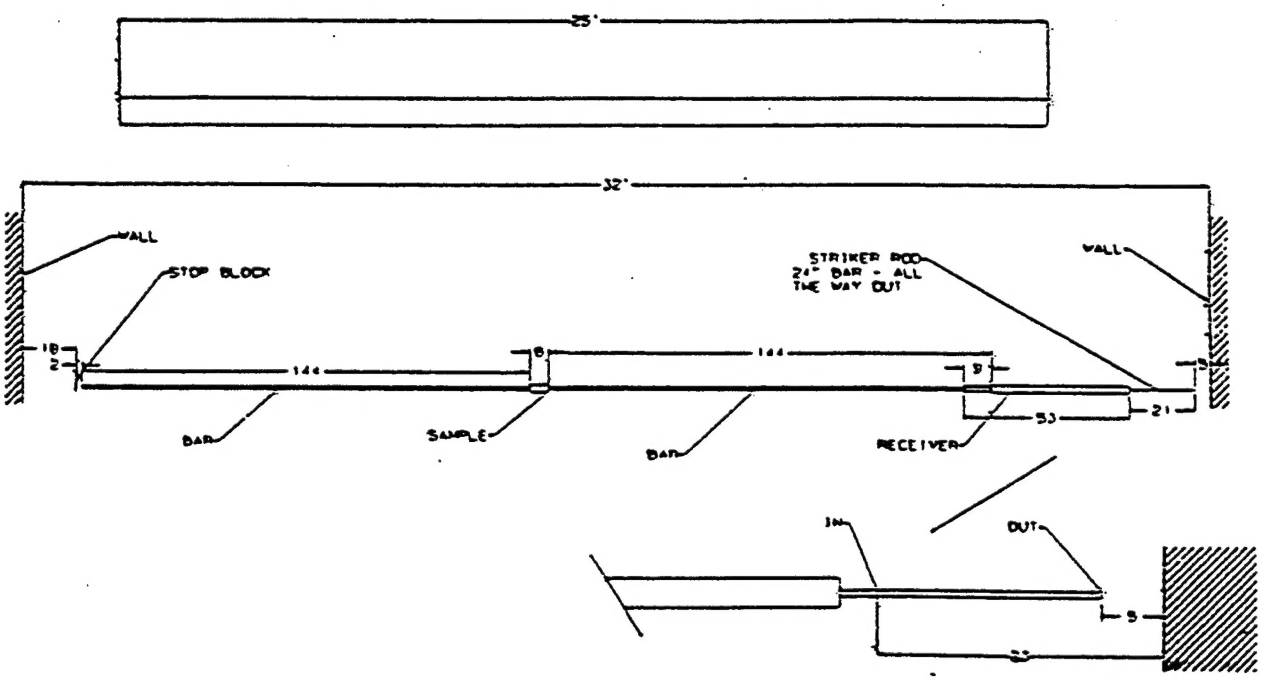

APPENDIX D

List of Publications in Preparation

D1: Experimental Determination and Modeling of Ballistic Limit of Graphite/Epoxy Laminate

D2: Effect of Thickness and Fiber Orientation on Nature of Damage

D3: Stress Wave Propagation and Effect of Stress Level on Penetration of Impact of Laminated Plate

D4: Characterization of Energy Expenditure and Mode of Failure of Laminated Graphite/Epoxy

D5: Modeling of Mixed-Mode failure Characterization of Laminated Plate

LAGRANGIAN X-T DIAGRAM OF STRESS PULSE WAVE PROPOGATION
IN SPLIT HOPKINSON BAR